JOURNAL OF GEOPHYSICAL RESEARCH: OCEANS, VOL. 118, 1–37, doi:10.1002/jgrc.20314, 2013

Hindcast and validation of Hurricane Ike (2008) waves, forerunner, and storm surge

M. E. Hope,[1] J. J. Westerink,[1] A. B. Kennedy,[1] P. C. Kerr,[1] J. C. Dietrich,[1,2] C. Dawson,[3] C. J. Bender,[4] J. M. Smith,[5] R. E. Jensen,[5] M. Zijlema,[6] L. H. Holthuijsen,[6] R. A. Luettich Jr.,[7] M. D. Powell,[8] V. J. Cardone,[9] A. T. Cox,[9] H. Pourtaheri,[10] H. J. Roberts,[11] J. H. Atkinson,[11] S. Tanaka,[1,12] H. J. Westerink,[1] and L. G. Westerink[1]

Received 26 February 2013; revised 9 July 2013; accepted 12 July 2013.

[1] Hurricane Ike (2008) made landfall near Galveston, Texas, as a moderate intensity storm. Its large wind field in conjunction with the Louisiana-Texas coastline's broad shelf and large scale concave geometry generated waves and surge that impacted over 1000 km of coastline. Ike's complex and varied wave and surge response physics included: the capture of surge by the protruding Mississippi River Delta; the strong influence of wave radiation stress gradients on the Delta adjacent to the shelf break; the development of strong wind driven shore-parallel currents and the associated geostrophic setup; the forced early rise of water in coastal bays and lakes facilitating inland surge penetration; the propagation of a free wave along the southern Texas shelf; shore-normal peak wind-driven surge; and resonant and reflected long waves across a wide continental shelf. Preexisting and rapidly deployed instrumentation provided the most comprehensive hurricane response data of any previous hurricane. More than 94 wave parameter time histories, 523 water level time histories, and 206 high water marks were collected throughout the Gulf in deep water, along the nearshore, and up to 65 km inland. Ike's highly varied physics were simulated using SWAN + ADCIRC, a tightly coupled wave and circulation model, on SL18TX33, a new unstructured mesh of the Gulf of Mexico, Caribbean Sea, and western Atlantic Ocean with high resolution of the Gulf's coastal floodplain from Alabama to the Texas-Mexico border. A comprehensive validation was made of the model's ability to capture the varied physics in the system.

Citation: Hope, M. E., et al. (2013), Hindcast and validation of Hurricane Ike (2008) waves, forerunner, and storm surge, *J. Geophys. Res. Oceans*, *118*, doi:10.1002/jgrc.20314.

1. Introduction

[2] The Louisiana and Texas (LATEX) Gulf Coast is situated in an area of high tropical storm activity. Major hurricanes making landfall along the LATEX coast include storms in 1886 (unnamed; landfall at Indianola, TX), 1900 (unnamed; landfall at Galveston, TX), 1915 (unnamed; landfall at Galveston, TX), 1961 (Carla), 1965 (Betsy), 1969 (Camille), 1980 (Allen), 1983 (Alicia), 2005 (Katrina and Rita), 2008 (Gustav and Ike), and 2012 (Isaac). Hurricane Ike is of significant interest because of its size, its varied response physics, and the quantity and quality of wave and water level data collected.

[3] Hurricane Ike entered the Gulf of Mexico after making landfall in Cuba. Upon entering the Gulf at 2030 UTC 9 September 2008 (Table 1), Ike tracked northwest and its wind field broadened and strengthened until reaching a 10 min sustained wind speed of 37 m s^{-1} and radius to maximum winds of 148 km at 0000 UTC 12 September 2008 (31 h before landfall), when the storm's center was approximately 300 km south of Isles Dernieres, LA (Figure 1, Table 2), with tropical storm force winds extending 400 km from the storm's center. At this point, significant wave heights were measured at over 8 m in the mid-Gulf, 6 m to the south of Grand Isle, LA, and 4 m off of Galveston Island. Approximately 13 h before

[1]Department of Civil and Environmental Engineering and Earth Sciences, University of Notre Dame, Notre Dame, Indiana, USA.
[2]Now at Department of Civil, Construction, and Environmental Engineering, North Carolina State University, Raleigh, North Carolina, USA.
[3]Institute for Computational Engineering and Sciences, University of Texas at Austin, Austin, Texas, USA.
[4]Taylor Engineering, Jacksonville, Florida, USA.
[5]Coastal and Hydraulics Laboratory, U.S. Army Engineer Research and Development Center, Vicksburg, Mississippi, USA.
[6]Faculty of Civil Engineering and Geosciences, Delft University of Technology, Delft, Netherlands.
[7]Institute of Marine Sciences, University of North Carolina at Chapel Hill, Chapel Hill, North Carolina, USA.
[8]Atlantic Oceanographic and Meteorological Labs, Hurricane Research Division, NOAA Miami, Florida, USA.
[9]Oceanweather Inc., Cos Cob, Connecticut, USA.
[10]New Orleans District, U.S. Army Corps of Engineers, New Orleans, Louisiana, USA.
[11]ARCADIS, Boulder, Colarado, USA.
[12]Now at Earthquake Research Institute, University of Tokyo, Tokyo, Japan.

Corresponding author: M. E. Hope, Department of Civil and Environmental Engineering and Earth Sciences, University of Notre Dame, 156 Fitzpatrick Hall, Notre Dame, IN 46556-5637. (mark.e.hope@gmail.com)

2169-9275/13/10.1002/jgrc.20314

Table 1. Summary of Significant Times and Characteristics of Hurricane Ike[a]

Hours Relative to Landfall	UTC Time	UTC Date (2008)	Latitude	Longitude	Max Wind Velocity (m/s)	Radius to Maximum Winds (km)	Minimum Central Pressure (mb)	Saffir-Simpson Category	Notes
−289	0600	1 Sep.	17.2	37	13	167	1006	Trop. Depression	Formation
−217	0600	4 Sep.	22.4	55.0	54	28	935	4	Maximum Intensity
−194.5	0430	5 Sep.	23.6	60.4	50	28	945	4	Enters SL18+TX33 Domain
−187	1200	5 Sep.	23.4	62.0	46	28	954	3	OWI winds start
−138	1300	7 Sep.	21.0	73.2	49		947	3	Landfall on Great Inagua Island, Bahamas
−124.75	0215	8 Sep.	21.1	75.7	50		945	4	Landfall in Holguin, Cuba
−89	1400	9 Sep.	22.6	82.9	30	-	965	1	Landfall in Pinar del Rio, Cuba
−82.5	2030	9 Sep.							Enters Gulf of Mexico
−31	0000	12 Sep.	26.1	90.0	37	148	954	2	
−19	1200	12 Sep.	26.9	92.2	39	93	954	2	Peak in South Plaquemines
−13	1800	12 Sep.	27.4	93.0	39	93	955	2	Shift in track, WSE peak in NOLA
−7	0000	13 Sep.	28.3	94.1	41	74	952	2	WSE peak in Lake Pontchartrain
0	0700	13 Sep.	29.3	94.7	41		950	2	Landfall at Galveston, Texas
5	1200	13 Sep.	30.3	95.2	37	56	959	1	
11	1800	13 Sep.	31.7	95.3	22	74	974	Trop. Storm	
23	0600	14 Sep.	35.5	93.7	15	93	986	Trop. Depression	OWI winds end
53	1200	15 Sep.							End of simulation

[a]Winds are 10 min average [*Berg*, 2009] (Automated Tropical Cyclone Forecast Archive: ftp://ftp.nhc.noaa.gov/atcf/).

landfall, Ike began to shift and track north-northwestward, then making landfall at Galveston Island, TX, with a maximum wind speed of 41 m s^{-1}. Ike generated a maximum measured surge at landfall of 5.3 m in Chambers County, TX, located to the northeast of Galveston Island (Figure 1) [*FEMA*, 2008]. Across the LATEX coast, Ike produced surge

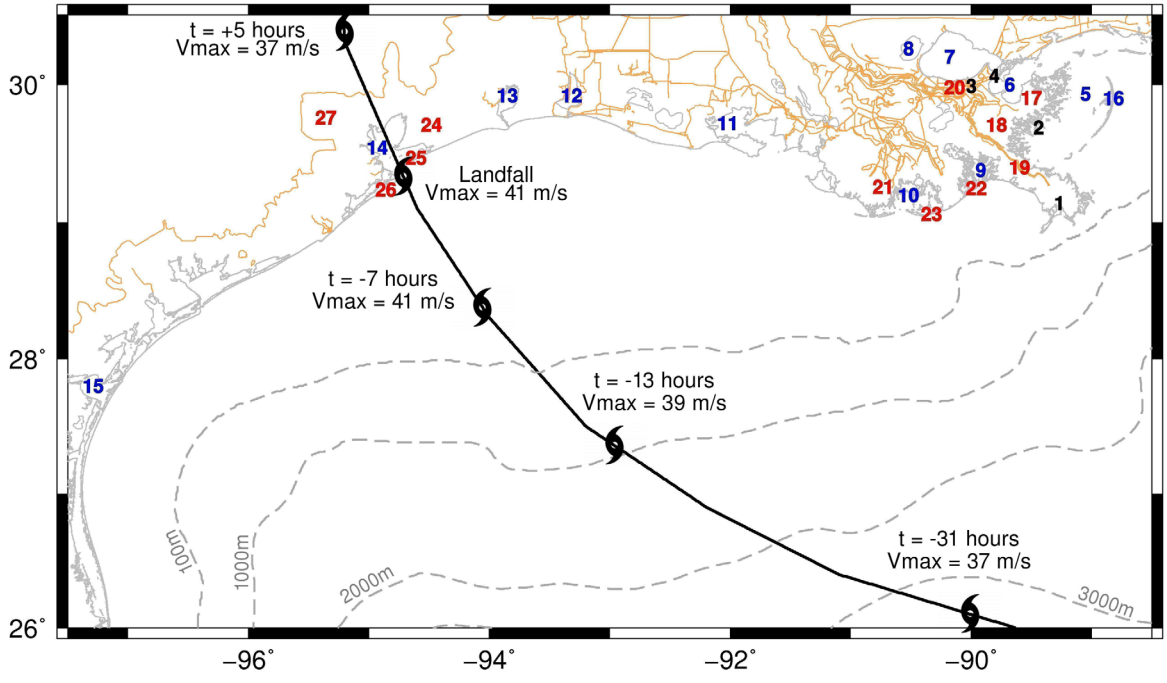

Figure 1. Map of Northern Gulf of Mexico and Louisiana-Texas Coast. The black line represents Ike's track; ADCIRC grid boundaries and raised features are brown; the coastline is solid gray; bathymetric contours (as labeled) are dashed gray. Geographic locations of significance are labeled by numbers identified in Table 2.

Table 2. Geographic Locations by Type and Location

	River and Channels
1	Mississippi River Bird's foot
2	Mississippi River Gulf Outlet (MRGO)
3	Inner Harbor Navigation Canal (IHNC)
4	Gulf Intracoastal Waterway (GIWW)
Water Bodies	
5	Chandeleur Sound
6	Lake Borgne
7	Lake Pontchartrain
8	Lake Maurepas
9	Barataria Bay
10	Terrebonne Bay
11	Vermillion Bay
12	Calcasieu Lake
13	Sabine Lake
14	Galveston Bay
15	Corpus Christi Bay
Locations	
16	Chandeleur Islands
17	Biloxi Marsh
18	Caernarvon Marsh
19	Plaquemines Parish, LA
20	New Orleans
21	Terrebonne Marsh
22	Grand Isle
23	Isles Dernieres, LA
24	Chambers County, TX
25	Bolivar Peninsula
26	Galveston Island
27	Houston, TX

levels of 1.8 m in Lake Pontchartrain, 2.2 m in Lake Borgne, 1.8 m at Grand Isle, 3.0 m near Vermillion Bay, LA, 4.5 m at the Sabine Lake Gulf Outlet, 3.3 m at Galveston Island, TX, and 1.5 m at Corpus Christi, TX.

[4] Following Hurricanes Katrina and Rita, wave and water level gages were strengthened to become more reliable under hurricane conditions. Additionally, the use of short-term deployable gages placed prestorm nearshore and inland increased the density of recorded data across the coast. As a result of these efforts, the number, density, and extent of wave and water level gages that collected data throughout the storm surpassed that of any previous storm.

[5] The wave measurements describe generation in deep water, transformation nearshore, and dissipation onshore and are summarized in Table 3.. NOAA National Data Buoy Center (NDBC; http://www.ndbc.noaa.gov/) wave data at 13 stations includes offshore buoys on the continental shelf as well as in the deep Gulf; Louisiana State University's Coastal Studies Institute (CSI; http://www.csi.lsu.edu/) recorded wave data at five nearshore gages off the coast of Southern Louisiana; Andrew Kennedy (AK) from the University of Notre Dame deployed eight gages via helicopter off the Texas coast from Sabine Lake to San Antonio Bay in depths ranging from 8.5 to 16 m [*Kennedy et al*., 2012]; the U.S. Army Corps of Engineers Research and Development Center Coastal Hydraulics Laboratory (USACE-CHL) deployed six gages in the Terrebonne and Biloxi marshes that were placed to understand the dissipation of waves over wetlands.

[6] Water level time series, Table 3., were collected throughout the LATEX shelf and adjacent floodplain by: the U.S. Army Corps of Engineers (USACE), the USACE-CHL, the National Oceanic and Atmospheric Organization (NOAA), the U.S. Geological Survey (USGS), the cooperative USGS and State of Louisiana Coastwide Reference Monitoring System (CRMS), CSI, the Texas Coastal Ocean Observation Network (TCOON), and AK. Time history data at these 523 stations describe in detail the development and evolution of surge on the LATEX shelf and its subsequent inland penetration. High water marks (HWMs) were collected for the Federal Emergency Management Agency (FEMA) following the storm. Of the available HWMs, data at 206 locations were deemed as reliable indicators of still-

Table 3.. Summary of Collected Data[a]

	Data Type							
Data Source	Water Levels	Significant Wave Height	Mean Wave Direction	Mean Wave Period	Peak Wave Period	High Water Mark	Winds	Currents
NDBC		13	9	13	13			
CSI	5	5	5	5	5	2		2
AK	8	8			8	8		
USACE-CHL	6	5			5	5		
NOAA	37					29	2	
USACE	38					33		
USGS-PERM	33					24		
USGS-DEPL	50					40		
TCOON	25					17	4	
CRMS	321					235		
TABS								4
FEMA						206		

[a]Data sources are as follows: NDBC, National Data Buoy Center (http://www.ndbc.noaa.gov/); CSI, Louisiana State University Coastal Studies Institute (http://www.csi.lsu.edu/); AK, University of Notre Dame, Andrew Kennedy [*Kennedy et al*., 2011a]; USACE-CHL, U.S. Army Corps of Engineers Coastal Hydraulics Laboratory (J. Smith, personal communication, 2009); NOAA, National Oceanic and Atmospheric Administration (http://tidesandcurrents.noaa.gov/); USACE, U.S. Army Corps of Engineers (http:// www.rivergages.com/; personal communication, 2011); USGS-PERM, U.S. Geological Survey (D. Walters, personal communication, 2009); (http://pubs.usgs.gov/of/2008/1365/); USGS-DEPL, U.S. Geological Survey [*East et al*., 2008]; TCOON, Texas Coastal Ocean Observation Network (http://lighthouse.tamucc.edu/TCOON/); CRMS, Coastwide Reference Monitoring System (http://www.lacoast.gov/crms2/); TABS, Texas Automated Buoy System (http://tabs.gerg.tamu.edu/); FEMA, Federal Emergency Management Agency [*FEMA*, 2008, 2009].

water elevations and resulting solely from Ike. An additional 393 water level time histories were identified as recording reliable still water high water levels. All water levels are referenced to the North American Vertical Datum of 1988 (NAVD88 2004.65 epoch in Louisiana).

[7] Wind data were used from four NOAA and two TCOON stations along the LATEX coast and current data were used from two CSI and four Texas Automated Buoy System (TABS; http://tabs.gerg.tamu.edu/) stations on the continental shelf.

[8] The measurement data provide a comprehensive description of Ike's waves and storm surge. Ike's expansive wave fields, with maximum measured significant wave heights reaching 10 m in the deep Gulf, were dominated by locally generated seas and well-defined swells that reached shore prior to the storm making landfall. Effective attenuation occurred on the continental shelf in the nearshore and especially behind barrier islands and within wetlands.

[9] Storm surge was dictated by geography, bathymetry, and storm track and included a variety of fundamentally different physical processes. Steady easterly winds across the Mississippi Sound and over the Biloxi and Caernarvon Marshes persisted as Ike was progressing across the Gulf of Mexico. This resulted in the effective capture of surge by the protruding Mississippi River Delta and river system, which projects onto the continental shelf. This slow process lasted 2 days, created a surge of 1.5–2.5 m in Lake Borgne and at the convergence of the Mississippi River Gulf Outlet (MRGO) and Gulf Intracoastal Waterway (GIWW). From this point, surge flowed into the Inner Harbor Navigation Canal (IHNC) into the heart of New Orleans peaking 13 h before landfall with a maximum water level of 2.5 m. This regional surge also drove water into Lakes Pontchartrain and Maurepas to the north of New Orleans through the Rigolets, Chef Menteur Pass, and Pass Manchac, where 1.8 m of surge was observed within Lake Pontchartrain, peaking 7 h before landfall. The same process occurred to the south and east of New Orleans in the marshes and wetlands of Plaquemines Parish. Water from Chandeleur Sound was pushed into the Caernarvon Marsh, reaching 3 m at English Turn. A 2 m surge was pushed from Breton Sound against the protruding west bank Mississippi River levee south of Point-a-la-Hache where there is no corresponding levee on the east bank [*Kerr et al*., 2013a, 2013b], peaking approximately 19 h before landfall. Having penetrated the river, this surge propagated upstream. The south and west facing portions of the "Bird's Foot" developed surge influenced by wave radiation stress gradient induced setup and moderate shore normal winds, and reached uniform levels of 1.2 m.

[10] The region from the Atchafalaya and Vermillion Bays to Galveston Bay was influenced by a geostrophically driven surge forerunner and by shore-perpendicular wind-driven surge. Water levels along this coast reached 2–2.5 m more than 12 h prior to landfall, while winds were still predominantly shore parallel or directed offshore. Factors controlling this Coriolis-driven early setup included: the wide LATEX shelf with its smooth muddy bottom, Ike's large size and steady northwest track, and the concave shape of the coast being coincident with the shore parallel winds [*Buczkowski et al*., 2006; *Kennedy et al*., 2011a, 2011b]. The time scale associated with the forerunner allowed surge to penetrate far inland into hydraulically connected water bodies and adjacent low lying coastal floodplains. For example, Morgan's Point within Galveston Bay and Manchester Point in the Houston Ship Channel experienced water levels of up to 2 m more than 12 h before landfall.

[11] The coastal forerunner propagated as a free continental shelf wave from Galveston, TX, southward on the LATEX shelf reaching Corpus Christi, TX, with an amplitude of 1.5 m. The time of arrival of the continental shelf wave at Corpus Christi, approximately 300 km southwest of Galveston, coincided with the landfall of the storm at Galveston. This was the largest measured continental shelf wave ever reported in the literature [*Kennedy et al*., 2011a, 2011b].

[12] The region between the Atchafalaya and Vermillion Bays and Galveston Bay also experienced a peak surge coincident to peak shore-normal winds ranging from 3 m adjacent to the Atchafalaya Bay, to 5 m to the west of Sabine Lake, and to 3.5 m near Galveston, TX. The forerunner-driven higher water levels within Galveston Bay persisted through the arrival of the strong winds at landfall, combining the forerunner and the wind-driven surge levels within and around the bay.

[13] As the storm passed and winds subsided, the coastal surge receded back onto the shelf. The abrupt bathymetric change at the continental shelf break led to an out-of-phase reflection of the surge back onto the shelf. The record shows a cross shelf wave appearing at the coast three times with increased damping with each cycle. The cross shelf wave has a period of approximately 12 h coinciding with the resonant period of the shelf. The resonant period of the shelf can also be seen in the strong amplification of semidiurnal tides on the wide portion of the LATEX shelf centered at Lakes Sabine and Calcasieu [*Mukai et al*., 2002].

[14] The scale and complexity of the Gulf, coastal features on the LATEX shelf, and the inland floodplain require the use of computational models that are basin-scale, multiprocess, and provide a high level of resolution in many areas. A coupled nonphase resolving wave and circulation model was used to simulate the waves, riverine driven flows, tides, and the wave-driven, wind-driven, and pressure-driven circulation during Ike. SWAN + ADCIRC is a tightly coupled modeling system that operates on an unstructured mesh, allowing for interaction of waves and circulation, and has recently been applied to hindcast Katrina, Rita, Gustav, and Ike [*Westerink et al*., 2008; *Dietrich et al*., 2011a, 2011b, 2012b]. As a means of comparison, ADCIRC has also been coupled to the Wave Model (WAM) and the Steady State Spectral Wave (STWAVE) model [*Komen et al*., 1994; *Smith*, 2000; *Smith et al*., 2001; *Günther*, 2005; *Smith*, 2007; *Bender et al*., 2013], which evaluate wave conditions on a sequence of structured grids throughout the Gulf and LATEX shelf and has been used to hindcast Katrina, Rita, and Gustav [*Bunya et al*., 2010; *Dietrich et al*., 2010, 2011a].

[15] For Ike, the SWAN + ADCIRC model uses the SL18TX33 computational domain that encompasses the western North Atlantic, Gulf of Mexico, and Caribbean Sea, and provides a very high level of resolution on the LATEX shelf and adjacent floodplain from Pensacola, FL, to the Texas-Mexico border. The SL18TX33 computational domain is an evolution of a sequence of earlier Louisiana

models with significant refinements in grid resolution and the incorporation of the entire Texas coastal floodplain [*Westerink et al*., 2008; *Bunya et al*., 2010; *Dietrich et al*., 2010, 2011a]. Nearshore and onshore, maximum element size is 200 m with a minimum of 20 m in channels and rivers. The continental shelf in the Gulf of Mexico is resolved with an element size of 500 m to 1 km increasing to 1–5 km in the deep Gulf of Mexico. The SL18TX33 mesh is an improvement over earlier studies, because high levels of resolution are extended from the southern Texas border through Mobile Bay, AL, and thus it describes the entire region that was affected as Ike moved onto the shelf and made landfall.

[16] Based on the unprecedented quality and quantity of measured event wave and water level data, the multitude of driver processes along the LATEX coast, the development of a highly resolved computational model of the entire LATEX coast and adjacent basins, and the availability of a high-resolution data-assimilated wind input field, Ike presents a unique and highly challenging opportunity to validate the performance of SWAN + ADCIRC. Model wave and water level responses will be qualitatively and quantitatively evaluated in comparison to measured data and put into context relative to the component physics.

2. Model Description

[17] Significant progress has been made in recent years to achieve full dynamic coupling of riverine flow, tides, atmospheric pressure, wind, and waves, in simulating hurricane waves and circulation. Basin-scale to inlet-scale domains incorporate basins, shelves, inland water bodies, channels, and floodplains, and require high spatial mesh variability in order to properly resolve processes at a local scale. Large, high-performance computing platforms with over 10,000 cores, in conjunction with highly scalable unstructured mesh codes, have allowed these improvements.

2.1. Wave and Surge Model

[18] ADCIRC was implemented for this simulation as a two-dimensional explicit barotropic model and solves the modified shallow water equations for water levels, ζ, and depth-averaged velocities in the x and y directions, U and V, respectively [*Kolar et al*., 1994; *Dawson et al*., 2006; *Westerink et al*., 2008; *Luettich and Westerink*, 2004, http://www.unc.edu/ims/adcirc/adcirc_theory_2004_12_08. pdf].

[19] Sufficient mixing on the continental shelf due to wave action has allowed for the two-dimensional, depth-integrated version of ADCIRC to be successfully applied. Observations in the Gulf during Hurricane Ivan (2004) indicate a well-mixed layer of 60 m during the passage of the storm [*Mitchell et al*., 2005]. Numerical studies suggest that turbulent mixing due to the interaction of winds, waves, and currents during Hurricane Frances (2004) in the upper ocean boundary layer extends down on the order of 100 m [*Sullivan et al*., 2012].

[20] The integrally coupled SWAN + ADCIRC model operates on a single unstructured mesh with ADCIRC solving for water levels and currents via the shallow water equations at a 0.5 s time step. ADCIRC passes these solutions to the unstructured implementation of SWAN, which solves the wave action balance equation, and passes wave radiation stresses back to ADCIRC [*Booij et al*., 1999; *Ris et al*., 1999; *Zijlema*, 2010; *Dietrich et al*., 2011b]. Information is exchanged every 600 model seconds, equivalent to the time step used in the SWAN computation. For the SWAN model, wave direction is discretized into 36 regular bins, frequency is logarithmically distributed over 40 bins ranging from 0.031384 to 1.42 Hz, wave growth mechanisms due to wind formulation is based on *Cavaleri and Rizzoli* [1981] and *Komen et al*. [1984], and modified whitecapping is based on *Rogers et al*. [2008]. In shallow water, depth-induced wave breaking is determined via *Battjes and Janssen*'s [1978] spectral model with the breaking index set to $\gamma = 0.73$ [*Battjes and Stive*, 1985]. These source term parameterizations are identical to recent studies using SWAN + ADCIRC [*Dietrich et al*., 2011a]. Within SWAN, spectral propagation velocities are limited in areas where insufficient mesh resolution may cause spurious wave refraction [*Dietrich et al*., 2012a, 2012b].

[21] Wave hindcasts are also performed with the WAM and STWAVE wave models coupled to ADCIRC. WAM is run on a Gulf-wide structured mesh and generates solutions that are forced as boundary conditions for STWAVE on a sequence of structured grids along the LATEX coast [*Komen et al*., 1994; *Smith*, 2000; *Smith et al*., 2001; *Günther*, 2005; *Smith*, 2007; *Bender et al*., 2013]. WAM is a third-generation model solving the action balance equation with 28 logarithmically distributed frequency bins and 24 equally spaced directional bins run on a structured Gulf-wide mesh with 0.05° resolution. WAM is run independently using default parameters, and its solution is used to specify the wave conditions at the boundary of the STWAVE nearshore wave model in conjunction with ADCIRC-generated winds and water levels. STWAVE uses a sequence of structured nearshore meshes with a resolution of 200 m. STWAVE solves the wave action balance equation using 45 frequency bins ranging from 0.0314 to 2.08 Hz and 72 equally spaced directional bins. The WAM/STWAVE + ADCIRC paradigm has demonstrated high skill in simulating nearshore waves and surge [*Bunya et al*., 2010; *Dietrich et al*., 2010]. Because of the loose coupling of ADCIRC to WAM/STWAVE, model duration is not required to coincide.

2.2. SL18TX33 Mesh

[22] The hindcast of Hurricane Ike applies the SWAN + ADCIRC model to the SL18TX33 computational mesh. The mesh domain includes the western North Atlantic Ocean, Caribbean Sea, Gulf of Mexico, and coastal floodplains of Alabama, Mississippi, Louisiana, and Texas (Figure 2). The mesh is the result of merging and refining two meshes, TX2008_R33 [*Kennedy et al*., 2011a, 2011b] and SL18, an evolution of the Louisiana SL16 mesh [*Dietrich et al*., 2011a]. Grid resolution varies from 20 km or larger in the deep Atlantic and Caribbean, 1–5 km in the central Gulf of Mexico, 1 km and lower on the continental shelf, 100–200 m in nearshore wave transformation zones, and as small as 20 m in channels and other similarly sized hydraulic features. The mesh consists of 9,108,128 nodes (vertices) and 18,061,765 triangular elements. At every computational node over the 600 s coupling interval, SWAN solves 1440 unknowns (36 directions, 40 frequencies every 600 s) for

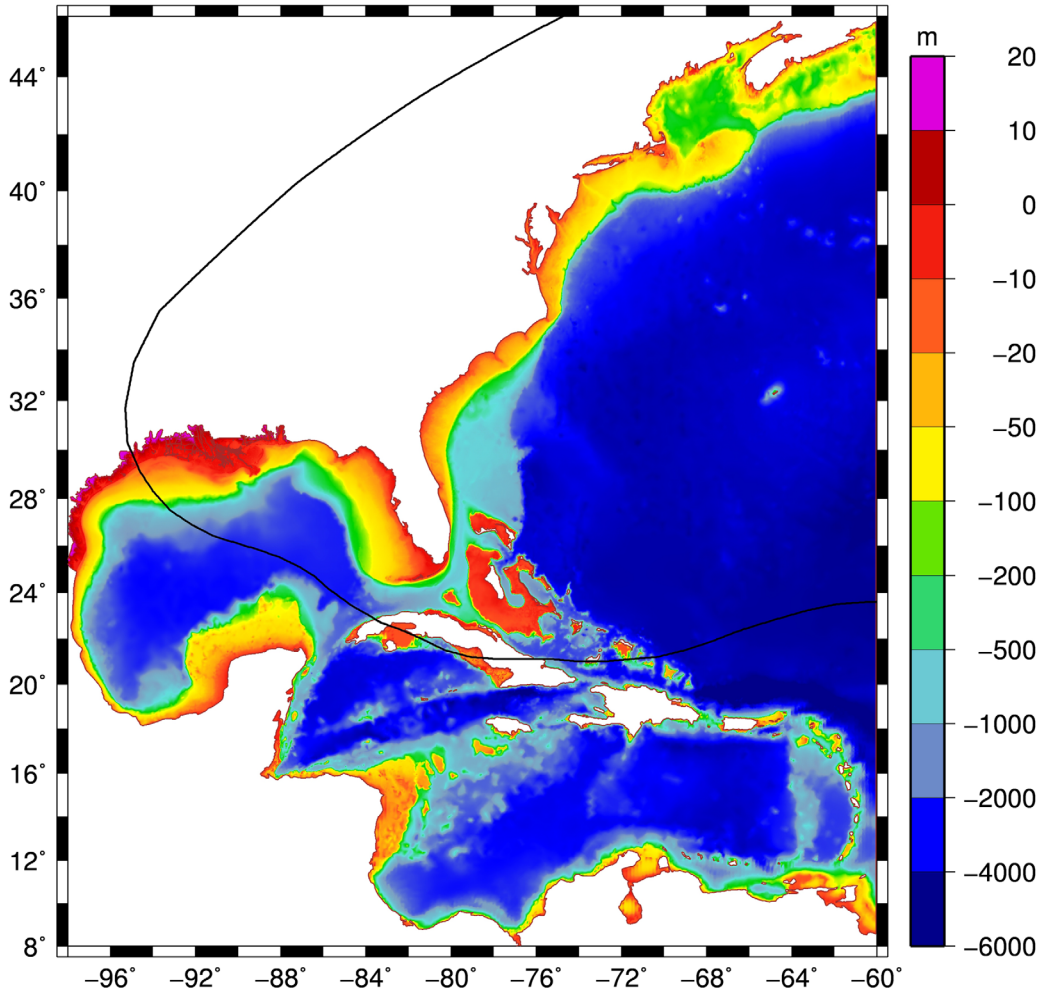

Figure 2. The SL18TX33 domain and grid bathymetry (m) of the SL18TX grid. Ike's track is shown with the black line for reference.

every 3600 ADCIRC unknowns (x and y direction currents and water level every 0.5 s).

[23] Bathymetric data for the Atlantic, Caribbean, and deep Gulf of Mexico was obtained from the ETOPO1 data set [*Amante and Eakins*, 2009]. Nearshore areas were specified using Coastal relief digital elevation models (http://www.ngdc.noaa.gov/mgg/coastal/), with data for inland water bodies including lakes, channels, and rivers coming from recent USACE and NOAA surveys. Marsh topography was specified based on marsh type with the Louisiana Gap Analysis Program (LA-GAP; http://atlas.lsu.edu/rasterdown.htm) land-cover databases with nonmarsh topography based on LiDAR (http://atlas.lsu.edu/lidar/) [*Dietrich et al*., 2011a]. In all cases, bathymetry/topography was applied to the mesh using a local element-scale averaging to avoid discontinuities. Relevant hydraulic barriers, such as levees, roads, and coastal dunes that lie below minimum mesh resolution, are represented in the mesh as lines of raised vertices or submesh-scale weirs [*Westerink et al*., 2008]. All coastal features are set to elevations consistent with post-Ike conditions. Bathymetric values and element sizes for the portion of the SL18TX33 domain that include the LATEX shelf and coast are depicted in Figures 3a and 3b.

[24] The use of the SL18TX33 mesh captures the basin, shelf-scale, and inland response physics of tides, waves, and surge generated by Ike. The broad spatial scale of the processes driven by Ike necessitates a computational domain encompassing the entire Gulf of Mexico and LATEX coast.

2.3. Winds

[25] Ike's core wind field was developed by NOAA's Hurricane Research Division Wind Analysis System (H*WIND). To create the wind field, data were assimilated from in situ monitoring systems (buoys and wind towers), remote sensing by satellites, and active measurement by aircraft [*Powell et al*., 1996, 1998, 2010]. H*WIND analysis is provided for an 8° × 8° area centered on the central position of the storm. H*WIND analysis is provided at 3 h intervals starting at 1930 UTC 5 September 2008 until 1630 UTC 13 September 2008. H*WIND analysis is blended with Gulf scale winds produced by the Interactive Kinematic Objective Analysis (IOKA) system [*Cox et al*., 1995; *Cardone and Cox*, 2009]. Final wind fields represent the conditions of 30 min sustained wind speeds at a height of 10 m with marine exposure. Gulf-wide winds are applied at a resolution of 0.1° with a finer resolution of 0.015° near

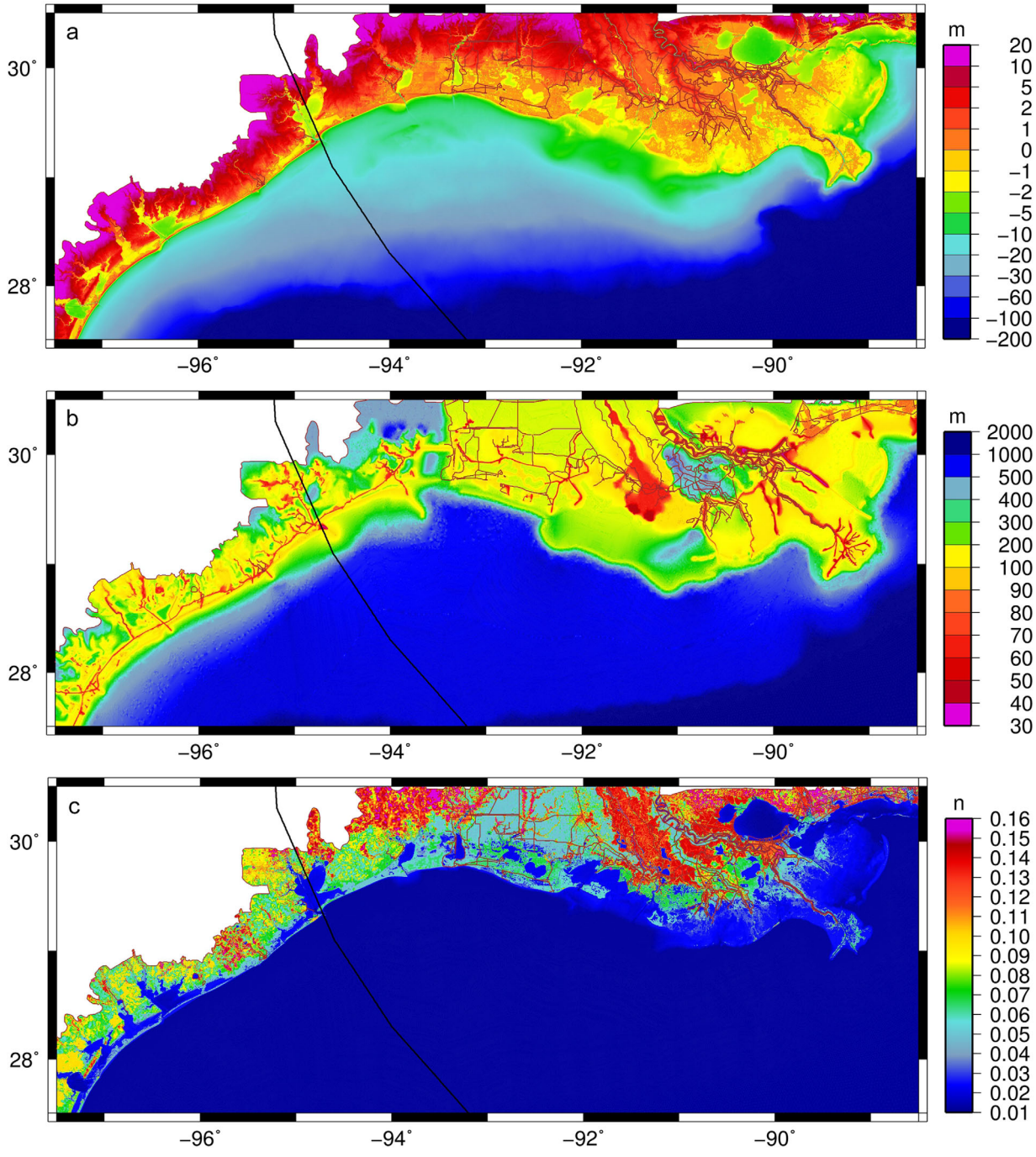

Figure 3. (a) Bathymetry/topography (m), (b) grid size (m), and (c) Manning's *n* of the SL18TX33 grid on the LATEX shelf and coast.

the landfall location. Final wind fields are provided at 15 min intervals starting at 1200 UTC 5 September 2008 until 0600 UTC 14 September 2008. It should be mentioned that the analyzed high resolution OWI H*WIND/IOKA data input into ADCIRC differs slightly from the data that appears in *Berg* [2009] resulting in slight discrepancies between modeled winds and reported winds.

[26] ADCIRC reads these marine wind fields and applies a wind gust factor of 1.09 to convert the 30 min sustained winds to 10 min sustained winds to be consistent with its air-sea drag formulation, as well as a directional wind reduction factor representing the reduction in 10 m wind speed as the atmospheric boundary layer evolves due to surface roughness on land [*Bunya et al.*, 2010]. ADCIRC applies a wind drag coefficient that is data-driven, wind speed limited, and directional [*Powell et al.*, 2003; *Powell*, 2006; *Dietrich et al.*, 2011a].

2.4. Vertical Datum Adjustment

[27] At the initiation of the simulation at 0000 UTC 8 August 2008, water levels are increased to correspond to the datum shift from local mean sea level to NAVD88 updated

to the 2004.65 epoch, to account for the intraannual sea surface variability driven by effects such as upper layer warming and seasonal riverine discharges, and the measured sea level rise from 2004 to 2008. The sea surface is raised 0.134 m to adjust computed values to NAVD88 2004.65 [*Garster et al*., 2007; *Bunya et al*., 2010] and 0.025 m due to sea level rise from 2004 to 2008. Then 0.121 m is added due to the intraannual variation, creating a total adjustment of 0.134 m + 0.025 m + 0.121 m = 0.280 m (http://tidesandcurrents.noaa.gov/sltrends/sltrends. shtml).

2.5. Bottom Friction

[28] Hydraulic friction is parameterized in the ADCIRC model using a spatially varying Manning's *n* value [*Bunya et al*., 2010]. These values are applied based on data supplied from the following land cover databases: LA-GAP, Mississippi Gap Analysis Program (MS-GAP; http://www.basic.ncsu.edu/segap/index.html), and the Coastal Change Analysis Program (C-CAP; http://www.csc.noaa.gov/digitalcoast/data/ccapregional/). The land classifications have standard Manning's *n* values associated with them that are assigned to the nodes via pixel averaging with values detailed in *Dietrich et al*. [2011a]. Offshore, areas with sandy/gravel bottoms such as the Florida shelf are set to $n = 0.022$ and areas with muddy bottoms like the LATEX shelf are set to $n = 0.012$ [*Buczkowski et al*., 2006]. The lower LATEX shelf friction is critical to developing fast flows that generate the large forerunner observed during the storm [*Kennedy et al*., 2011a, 2011b]. These values are applied at depths >5 m, and they are increased linearly to $n = 0.022$ toward the shoreline. Manning's *n* values for a portion of the SL18TX33 domain including the LATEX shelf and coast are depicted in Figure 3c.

[29] SWAN utilizes a roughness length formulated by *Madsen et al*. [1988] based on Manning's *n* values used in ADCIRC and water depths computed in ADCIRC:

$$z_0 = H\exp\left[-\left(1+\frac{\kappa H^{1/6}}{n\sqrt{g}}\right)\right]$$

where $\kappa = 0.4$ (Von Karman constant), H = total water depth computed in ADCIRC, and g = gravitational constant [*Bretschneider et al*., 1986]. SWAN computes a new roughness length at each time step based on updated ADCIRC water level values. To avoid unrealistically small roughness length values, the minimum Manning's *n* value passed to SWAN is $n = 0.02$ (minimum *n* is set to 0.03 for STWAVE).

2.6. Rivers

[30] River inflow into the domain occurs at two locations: Baton Rouge, LA, representing the Mississippi River and Simmesport, LA, representing the Atchafalaya River. Both locations use a river-wave radiation boundary condition in order to allow tides and storm surge to propagate upstream past these boundaries [*Westerink et al*., 2008; *Bunya et al*., 2010]. River flow is ramped up from zero using a hyperbolic ramp function for a period of 0.5 days. Following the ramping period, river levels are given 3 days to reach equilibrium. After 3.5 days, river levels at the inflow boundaries are held constant and tidal forcing commences, with meteorological forcing starting at a later specified time. River discharges were determined using data from the US Army Corps of Engineers New Orleans District (http://www.mvn.usace.army.mil) for the period between 5 September 2008 and 15 September 2008. River flow rates used were 12,210 m^3/s and 5233 m^3/s for the Mississippi and Atchafalaya Rivers, respectively.

2.7. Tides

[31] Periodic conditions are applied at the open ocean boundary along the 60°W meridian. Astronomical tides (K_1, O_1, Q_1, P_1, M_2, S_2, N_2, and K_2) are forced on the open ocean boundary using the TPXO7.2 tidal atlas [*Egbert et al*., 1994; *Egbert and Erofeeva*, 2002]. Nodal factors and equilibrium arguments are computed and applied for the simulation start time. Tides are ramped using a hyperbolic tangent function for 12 days to avoid exciting spurious modes in the resonant Gulf of Mexico and Caribbean Sea basins, reaching full amplitude 2.5 days before the start of meteorological forcing.

3. Recorded Data

[32] Following Katrina and Rita, existing gages were strengthened to assure data records were produced for the duration of tropical storms. Additionally, temporary gages were placed in nearshore areas such as marshes, creeks, and 1–5 km offshore to produce a composite understanding of wave and surge generation, evolution, and dissipation, and provide a wealth of validation data (Table 3.). Each time series was reviewed and assessed for accuracy and reliability, with range limited or failed periods of data being removed to assure appropriate comparison to model solutions.

4. Synoptic History and Validation

[33] The evolution of Hurricane Ike winds, waves, and surge fields, as simulated by the coupled SWAN+ADCIRC model, and qualitative and quantitative comparisons to data using the extensive wave and water level data are presented. The simulation is started from a cold start on 0000 UTC 8 August 2008, with a 3.5 day riverine spin-up period allowing river levels to reach equilibrium followed by a 12 day tidal spin allowing the tides in the Gulf of Mexico to attain a dynamic equilibrium. A 10.5 day Gustav simulation is run from 0000 UTC 26 August 2008 to 1200 UTC 5 September 2008 to establish ambient water level conditions prior to Ike, which is simulated over a 10 day period from 1200 UTC 5 September 2008 to 1200 UTC 15 September 2008. Wind, wave, water level, and current fields throughout the period of 18 h prior to landfall to 12 h after landfall are shown in Figures 4–8. Time series and locations of select wind, wave, water level, and current stations are presented in Figures 9–25.

4.1. Winds

[34] Ike crossed the 60°W meridian at 0430 UTC 5 September 2008, entering the SL18TX33 domain. Before entering the Gulf of Mexico, Ike made landfall in eastern and western Cuba. Upon entering the Gulf, at 2030 UTC 9 September 2008, Ike moved northwest and grew in size [*Berg*, 2009]. Tropical storm force winds (10 min sustained surface winds of at least 15 m s^{-1}) first reached the Mississippi River Delta in Southern Louisiana at 1500 UTC 11

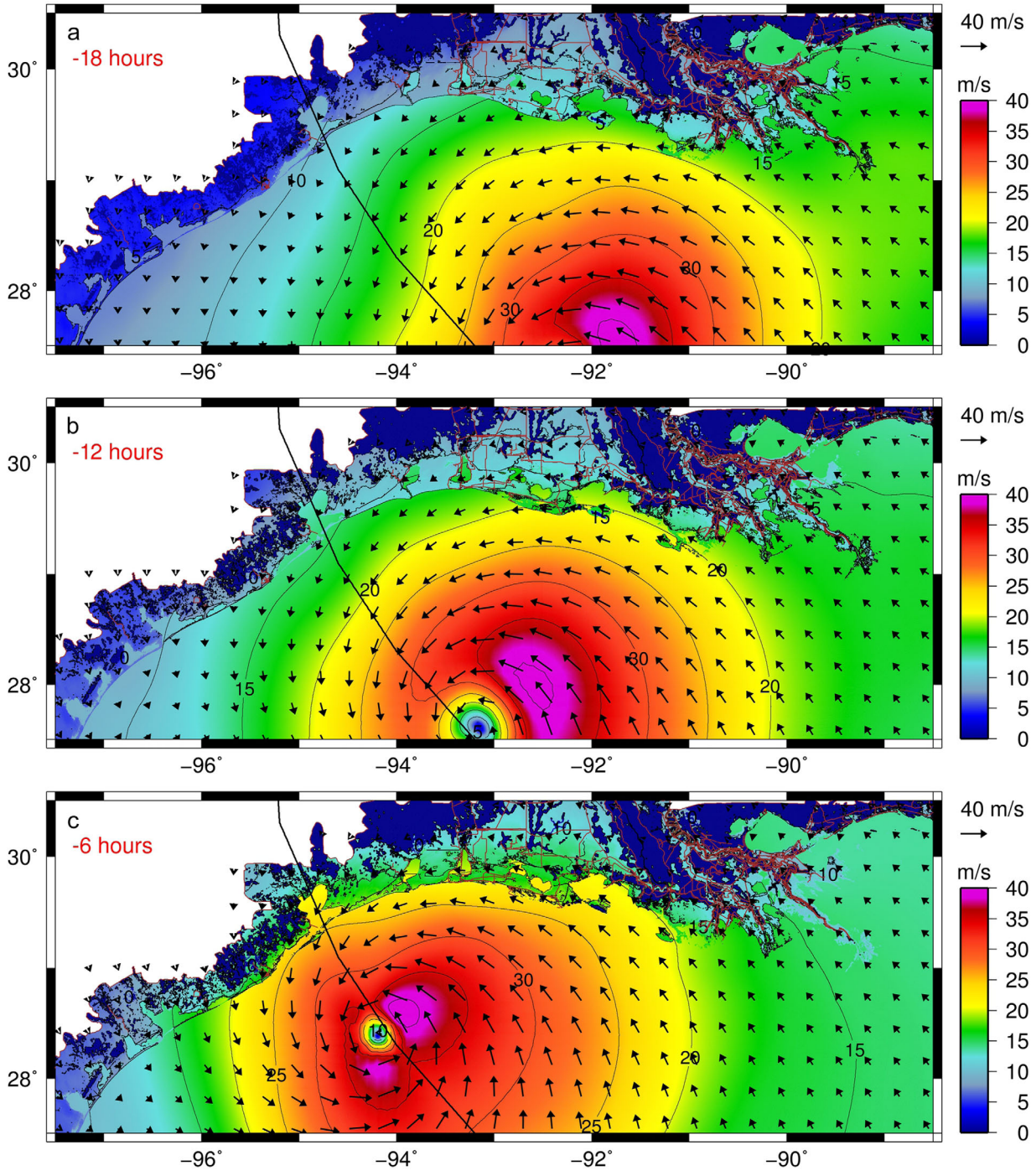

Figure 4. Wind speeds m s^{-1} on the LATEX shelf and coast during Ike. Vectors representing wind speed and direction are displayed. Plots represent the following times: (a) 1300 UTC 12 September 2008, approximately 18 h before landfall, (b) 1900 UTC 12 September, approximately 12 h before landfall, (c) 0100 UTC 13 September, approximately 6 h before landfall, (d) 0700 UTC 13 September, approximately at landfall, (e) 1300 UTC 13 September, approximately 6 h after landfall, and (f) 1900 UTC 13 September, approximately 12 h after landfall.

September 2008, 40 h before landfall, and persisted for more than 36 h. Winds over the Mississippi, Breton, and Chandeleur Sounds were consistently easterly and southeasterly and directed toward the protruding Mississippi River Delta, significantly impacting surge development in the region. According to OWI H*WIND/IOKA reanalysis, Ike reached its peak wind speed of 41 m s^{-1} in the Gulf of Mexico at 0430 UTC 12 September 2008. At this point, Ike's tropical storm force and stronger winds produced an integrated kinetic energy of 154 TJ corresponding to a 5.4 out of a possible 6 on the Surge Destructive Potential Scale [*Powell and Reinhold*, 2007], with tropical storm force winds and

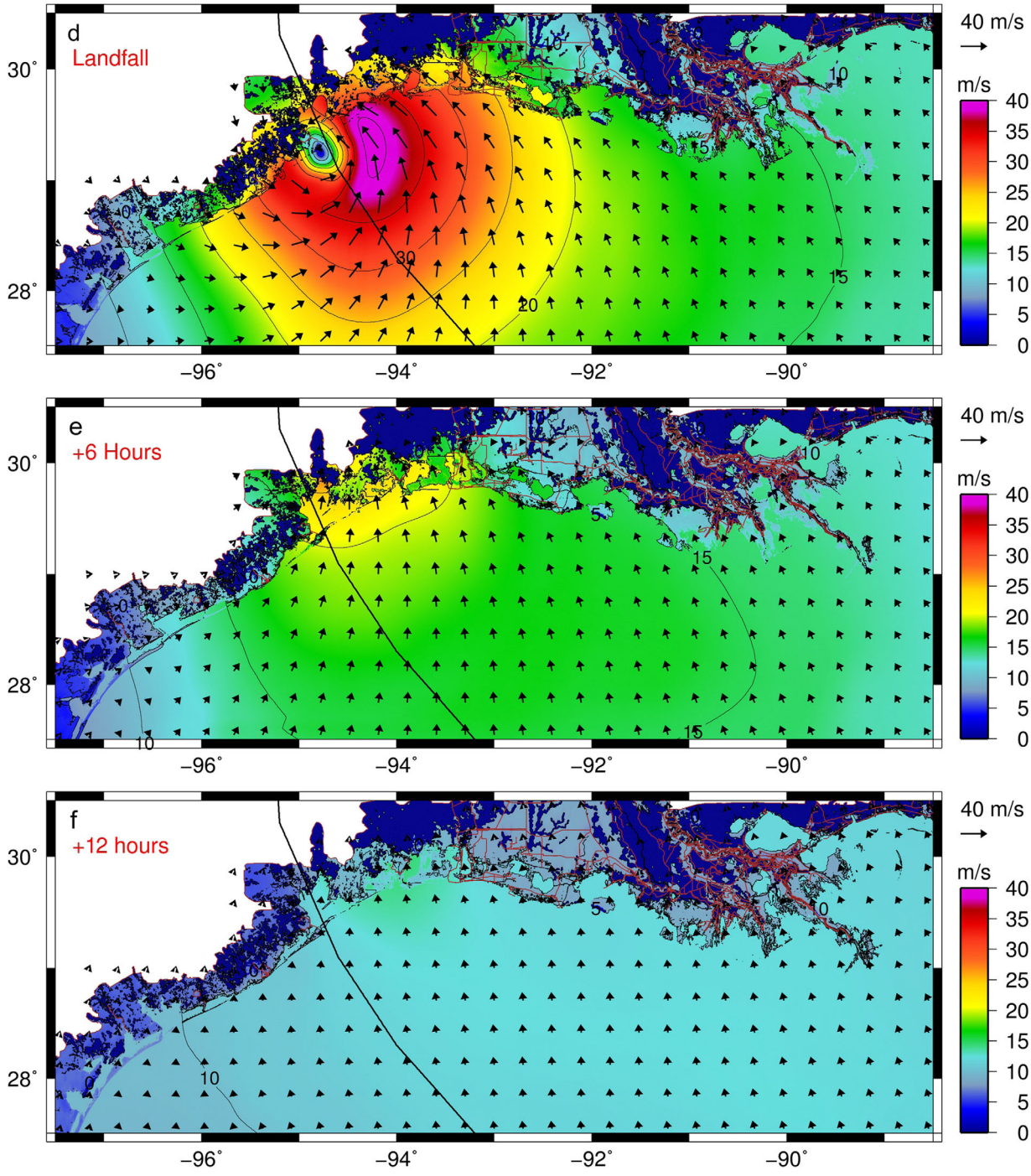

Figure 4. (continued)

hurricane force winds extended out 400 km and 140 km, respectively, from the center of the hurricane. After slightly weakening later on 12 September 2008, Ike would again reach a peak wind speed of 41 m s^{-1} before and at landfall at Galveston, TX, at 0700 UTC 13 September 2008.

[35] During the period from 1300 UTC 12 September 2008, 18 h prior to landfall, until 0100 UTC 13 September 2008, 6 h prior to landfall, much of the LATEX shelf and coast experienced shore-parallel winds as a result of the large size of the storm and large-scale circular coastal geography of the region, Figures 4a–4c. Winds shifted slowly as the storm progressed, and areas in the immediate vicinity of landfall, such as Galveston Island and the Bolivar Peninsula, did not experience a shift in wind direction until immediately before the storm's center had made landfall. At landfall (Figure 4d), Ike's maximum wind speed was 41 m s^{-1} occurring at the coast of the Bolivar Peninsula. As Ike approached the coast and made landfall, winds transitioned to shore-normal orientation, blowing onshore northeast of landfall and offshore southwest of landfall. The storm tracked through the east side of Galveston Bay, which at landfall was already filled with more than 2 m of additional

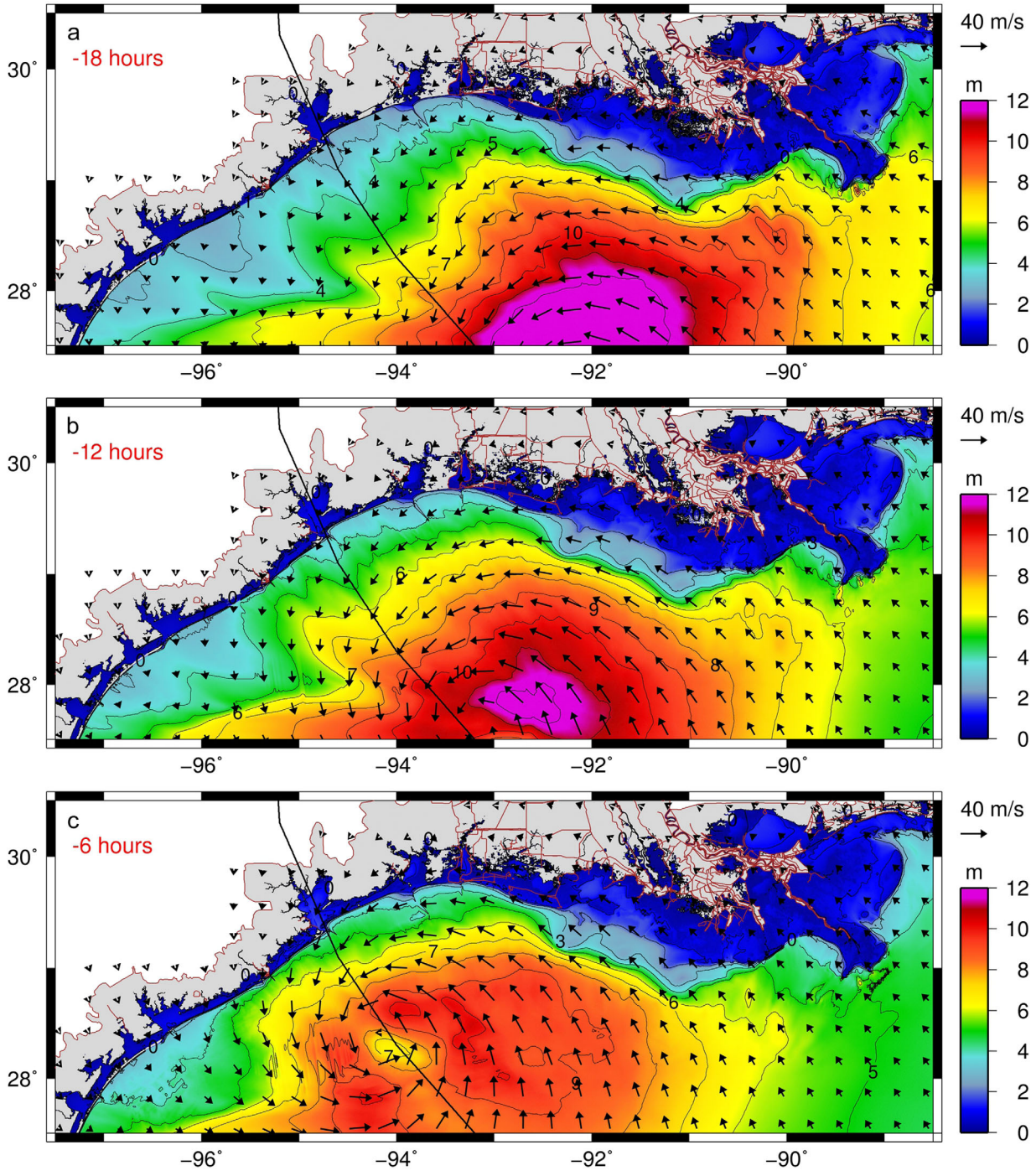

Figure 5. SWAN significant wave heights (m) on the LATEX shelf and coast during Ike. Vectors representing wind speed and direction are displayed. Plots represent the following times: (a) 1300 UTC 12 September 2008, approximately 18 h before landfall, (b) 1900 UTC 12 September, approximately 12 h before landfall, (c) 0100 UTC 13 September, approximately 6 h before landfall, (d) 0700 UTC 13 September, approximately at landfall, (e) 1300 UTC 13 September, approximately 6 h after landfall, and (f) 1900 UTC 13 September, approximately 12 h after landfall.

water caused by the forerunner surge and was impacted by near-maximum-strength winds before landfall and 30 m s^{-1} winds immediately after landfall.

[36] Following landfall, winds over Galveston Bay and in the area of landfall remained oriented onshore. Six hours after landfall winds over Galveston Bay were 20 m s^{-1}, still tropical storm force (Figure 4e). These persistent onshore winds impeded the recession of water out of Galveston Bay and the marshes to the northeast of Bolivar Peninsula where maximum recorded water levels during Ike occurred.

[37] Figure 9 shows the locations of six observation stations on the LATEX shelf and onshore that recorded wind

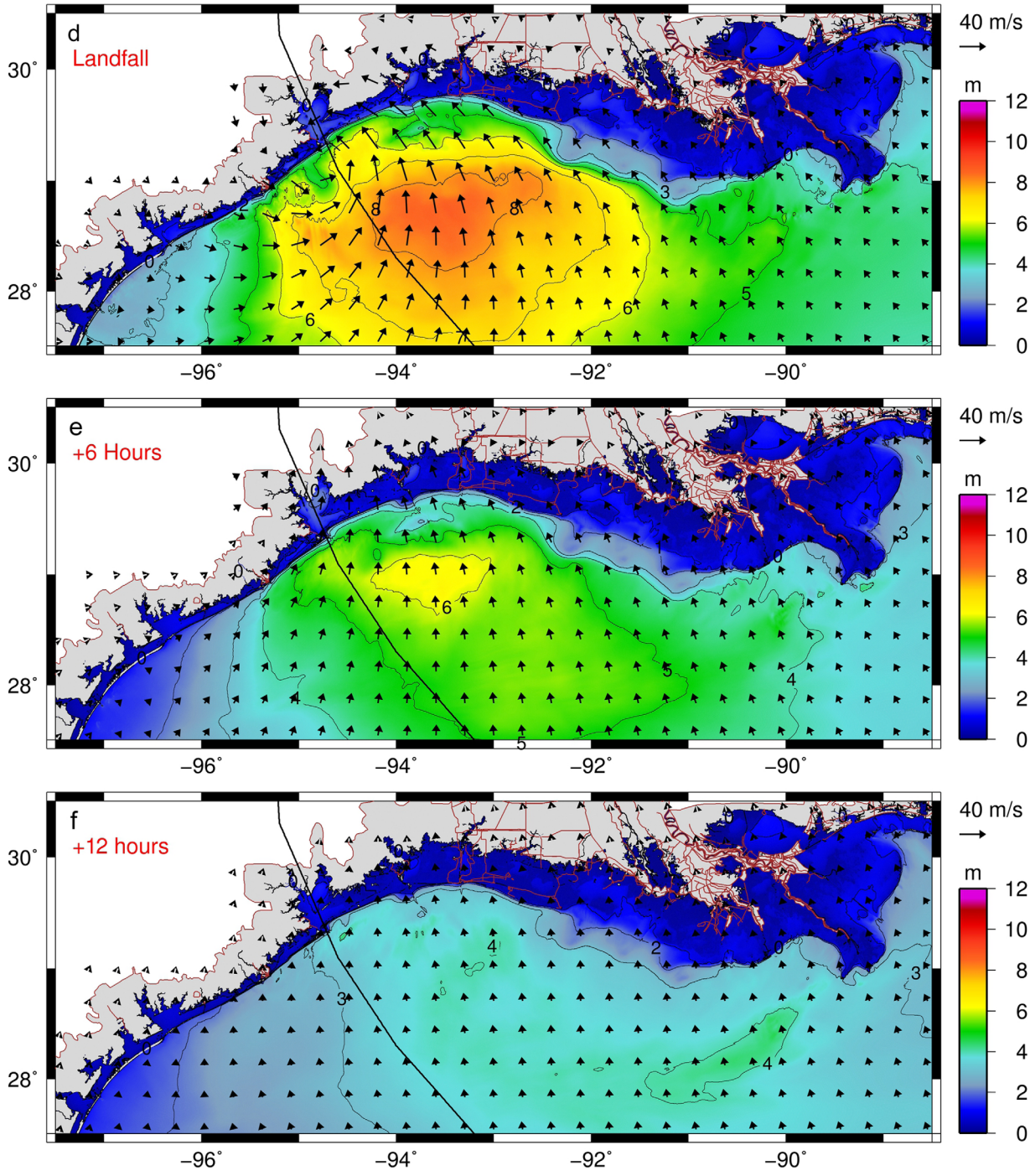

Figure 5. (continued)

velocity and direction during Hurricane Ike. Figures 10 and 11 compare the OWI H*WIND/IOKA-based wind speeds and directions as adjusted by ADCIRC (10 min average winds; overland directional wind boundary layer adjustments; adjustment for water column height relative to physical roughness element scale) to the observed data. Unfortunately, many data recording stations failed at or before peak winds near landfall, leaving fewer points of comparison for the maximum winds. It should be noted that the OWI wind fields used as ADCIRC input represent large-scale synoptic wind patterns and exclude local and short time scale phenomena, such as the diurnal cycle seen in the observed data. This diurnal cycle is particularly prominent at station TCOON 87730371. In regard to the synoptic cyclonic winds, the OWI winds capture well the growth, peak, and reduction of wind velocities. Of particular note is the capture of the passing of the eye at station TCOON 87710131. One particular source of error in the OWI winds is the underprediction of winds on the LATEX shelf before landfall, as seen in stations TCOON 87713411 and TCOON 87710131 between 3 and 15 h GMT on 12 September. These moderate velocity shelf parallel winds

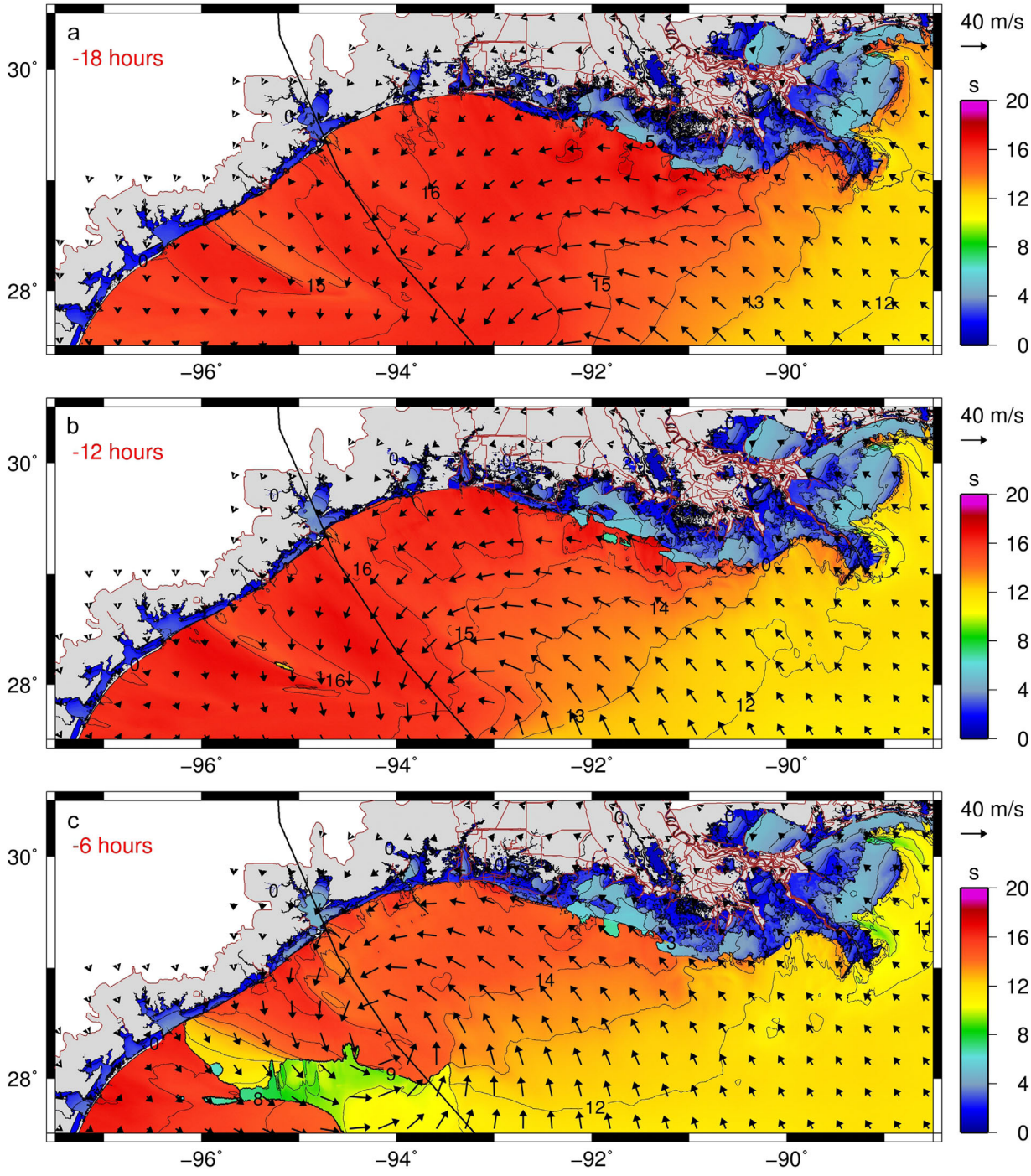

Figure 6. SWAN peak period (s) on the LATEX coast during Ike. Vectors representing wind speed and direction are displayed. Plots represent the following times: (a) 1300 UTC 12 September 2008, approximately 18 h before landfall, (b) 1900 UTC 12 September, approximately 12 h before landfall, (c) 0100 UTC 13 September, approximately 6 h before landfall, (d) 0700 UTC 13 September, approximately at landfall, (e) 1300 UTC 13 September, approximately 6 h after landfall, and (f) 1900 UTC 13 September, approximately 12 h after landfall.

drive the forerunner surge and underprediction of these winds leads to a lower shore parallel current and lower water levels prelandfall. In regard to wind direction, the OWI winds capture the shifting of winds as Ike made landfall, but fail to capture some of the short-time scale shifts in wind direction. Because these short-duration localized phenomena are not captured in the OWI winds, they will not appear in the ADCIRC circulation response.

4.2. Waves

[38] As Ike progressed through the Gulf of Mexico, the largest waves were generated by the storm's most intense

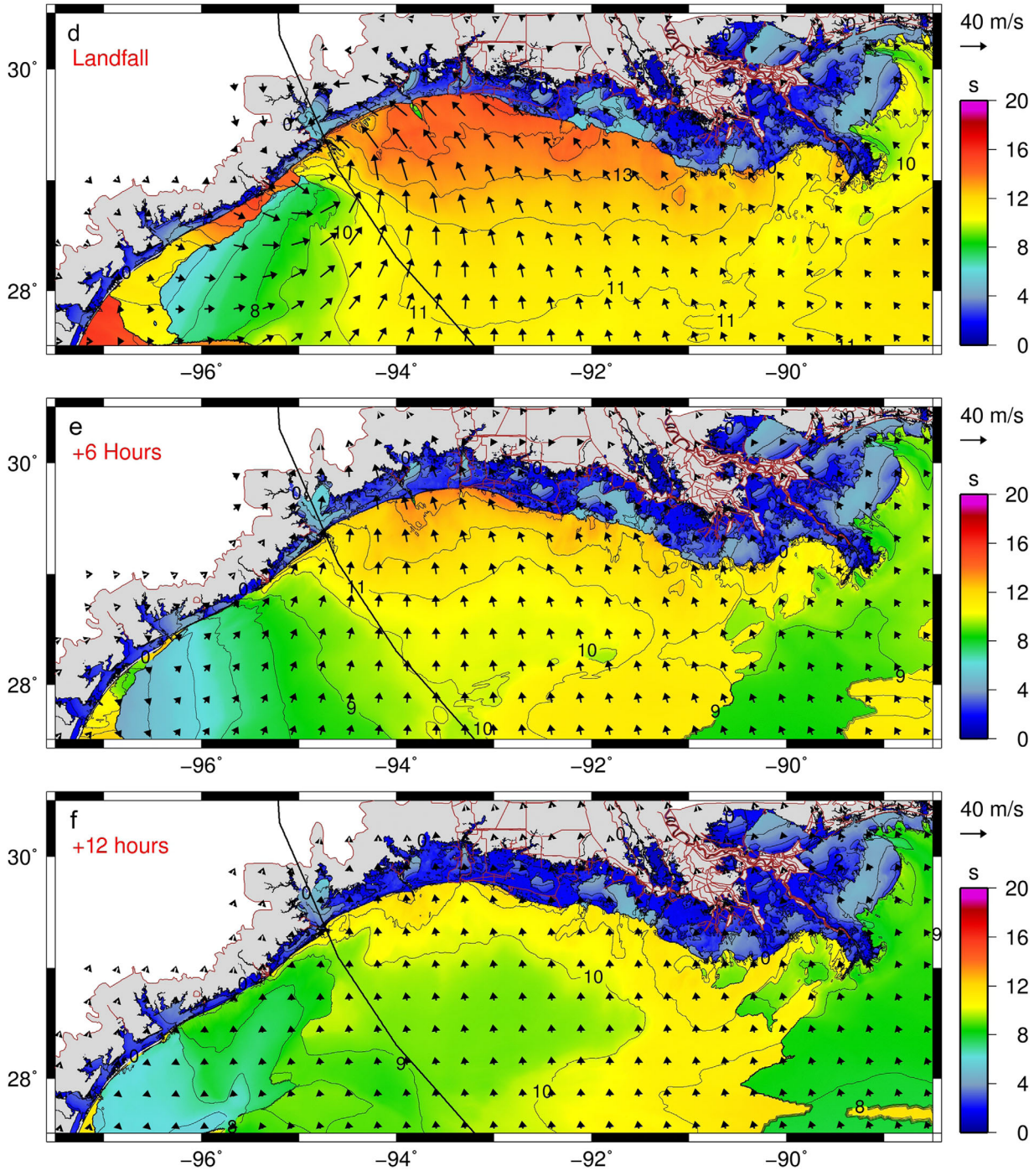

Figure 6. (continued)

winds located to the east of the eye, as illustrated in Figures 5 and 6. In the northeastern Gulf, deep water NDBC buoys 42036 and 42039 recorded significant wave heights of 4 m and 8 m, respectively, and maximum mean wave periods of 10 s and 12 s, respectively (Figures 12–14). Ike passed just to the east of NDBC buoy 42001, generating a maximum significant wave height of almost 10 m before the storm passed and 8 m afterward with a maximum mean period of 12 s as the storm center passed over the buoy (Figures 12–14). Maximum computed SWAN significant wave heights in the Gulf of Mexico exceeded 15 m, occurring in the deep Gulf to the south of the Louisiana continental shelf break. Far to the west of the track at NDBC buoys 42002 and 42055, significant wave heights reached 6 m and 3 m, respectively, and mean periods reached 13 s at both buoys (Figures 12–14).

[39] To the east of New Orleans on the Alabama-Mississippi Shelf, the shallow bathymetry and the associated depth-limited breaking attenuated the large ocean swell (Figures 5 and 6). Furthermore, the Chandeleur Islands prevented these large, long waves from entering the Chandeleur Sound, limiting wave heights in the Sound to

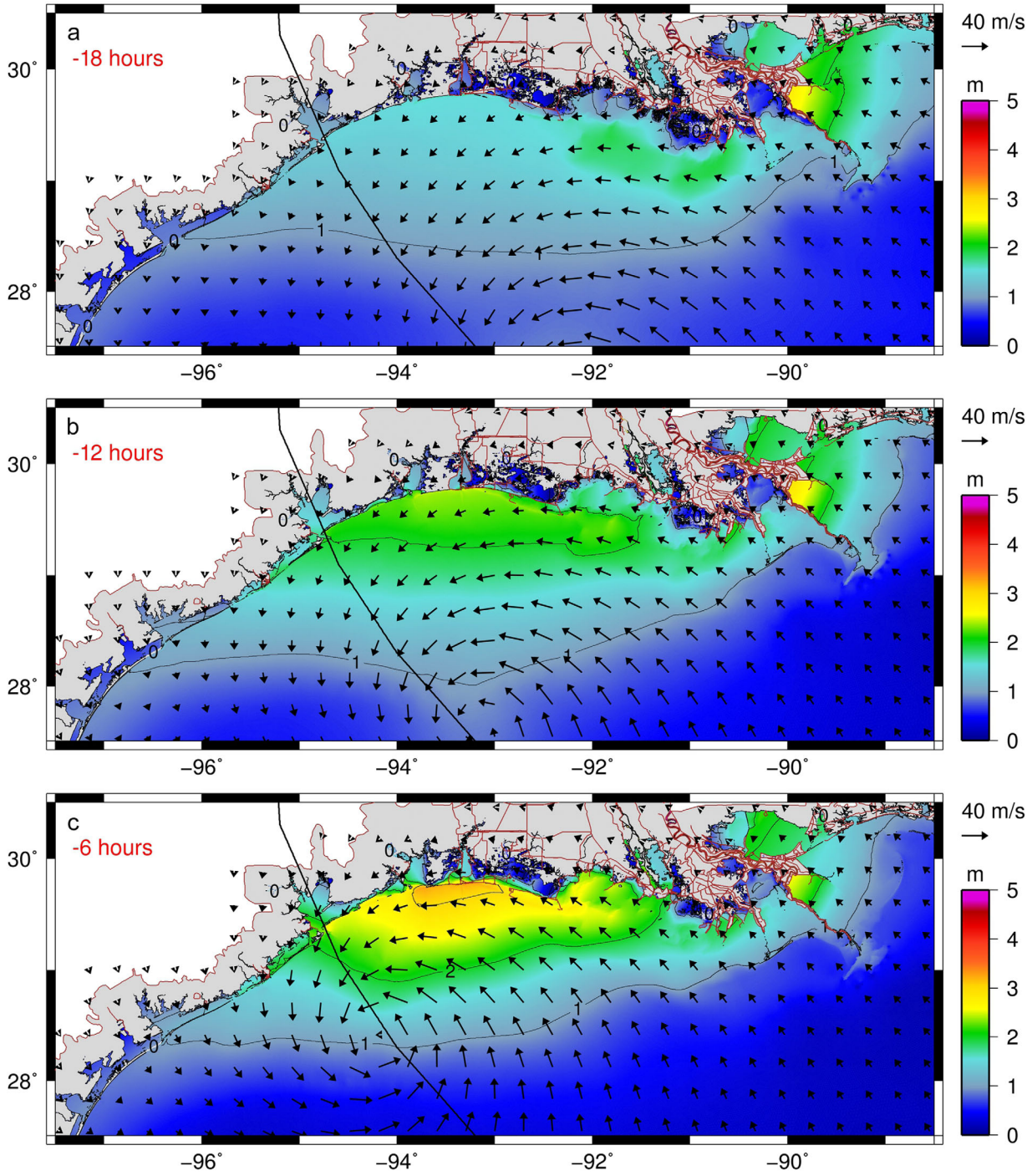

Figure 7. ADCIRC water surface elevation (m) on the LATEX shelf and coast during Ike. Vectors representing wind speed and direction are displayed. Plots represent the following times: (a) 1300 UTC 12 September 2008, approximately 18 h before landfall, (b) 1900 UTC 12 September, approximately 12 h before landfall, (c) 0100 UTC 13 September, approximately 6 h before landfall, (d) 0700 UTC 13 September, approximately at landfall, (e) 1300 UTC 13 September, approximately 6 h after landfall, and (f) 1900 UTC 13 September, approximately 12 h after landfall.

<2 m. In the Biloxi Marsh, friction and even shallower depths limited wave heights to 0.5 m and peak periods to 5 s. This rapid transformation from deep water to land is observed by NDBC buoys 42040 and 42007, and CHL gages 2410510B, 2410513B, and 2410504B (Figures 12–16 and 17).

[40] The narrow shelf to the south and west of the Mississippi River Delta allows large swell waves to propagate close to the delta and bays to the west (Figures 5 and 6). Rapid wave attenuation occurs as depths become shallow and wetlands are penetrated. Offshore from Terrebonne Bay, CSI gages 06 and 05 recorded significant wave

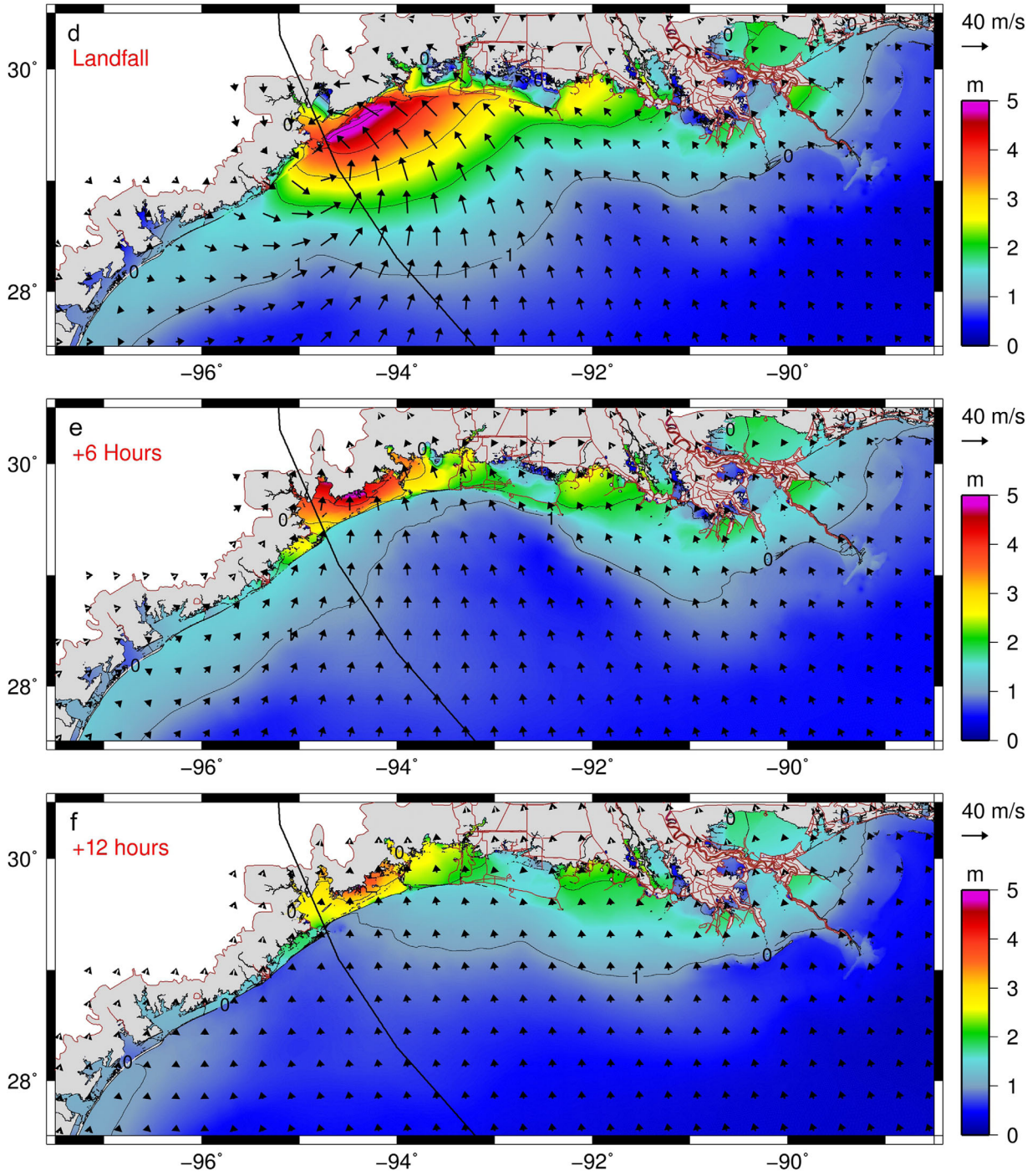

Figure 7. (continued)

heights of 6 m and 3 m, respectively, and a maximum peak wave period of 16 s (Figures 12, 16, and 17). CHL wave gage 2410512B in the marshes to the north of Terrebonne Bay recorded significant wave heights of 1 m and peak wave periods reached a maximum of 3 s, demonstrating the depth limited and bottom friction induced breaking that occurs in the bay and marsh system.

[41] The broad Texas shelf also limited the propagation of the large swell waves generated in the central deep Gulf (Figures 5 and 6). NDBC buoys 42019 and 42020 are both positioned on the outer Texas shelf southwest of landfall and recorded significant wave heights of up to 7 m and maximum mean wave periods of 12 s and 14 s, respectively. On the inner Texas shelf, NDBC buoy 42035 (which was dislodged from its mooring as the storm passed; http://www.ndbc.noaa.gov/station_page.php?station=42035) was initially located just to the south of Ike's track and recorded a significant wave height of 6 m and maximum mean wave period of 13 s before being dislodged in the hours before Ike passed. On the nearshore Texas shelf, Andrew Kennedy's (AK) gages, Z, Y, X, W, V, S, and R, shown in Figures 12, 16, and 17, recorded wave heights and peak periods in mean

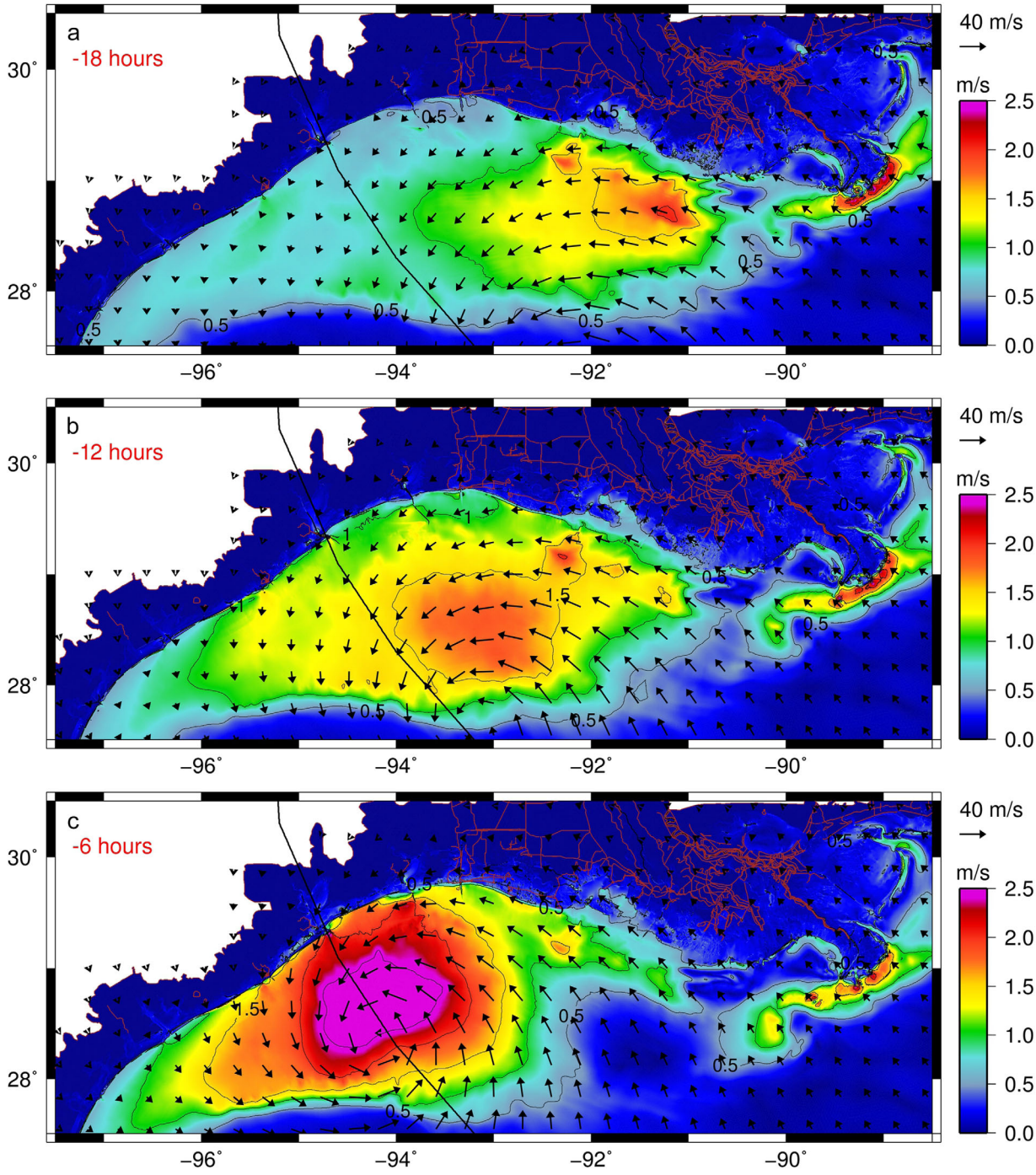

Figure 8. ADCIRC currents (m s^{-1}) on the LATEX shelf and coast during Ike. Vectors representing wind speed and direction are displayed. Plots represent the following times: (a) 1300 UTC 12 September 2008, approximately 18 h before landfall, (b) 1900 UTC 12 September, approximately 12 h before landfall, (c) 0100 UTC 13 September, approximately 6 h before landfall, (d) 0700 UTC 13 September, approximately at landfall, (e) 1300 UTC 13 September, approximately 6 h after landfall, and (f) 1900 UTC 13 September, approximately 12 h after landfall.

water depths of 8.5–16 m covering a section of coast from Bolivar Peninsula north of landfall to Corpus Christi south of landfall. Stations AK Z and Y to the north of landfall experienced the strongest landfalling winds and recorded significant wave heights of 5 m and peak wave periods of 16 s prior to landfall and 6–12 s at landfall indicating the transition from swell dominance to wind-sea dominance as Ike passed. To the south of landfall, AK stations X, V, S, and R (Figure 12) recorded maximum significant wave heights of 5.8 m, 5 m, 3 m, and 4.5 m, respectively (Figure 16). Based

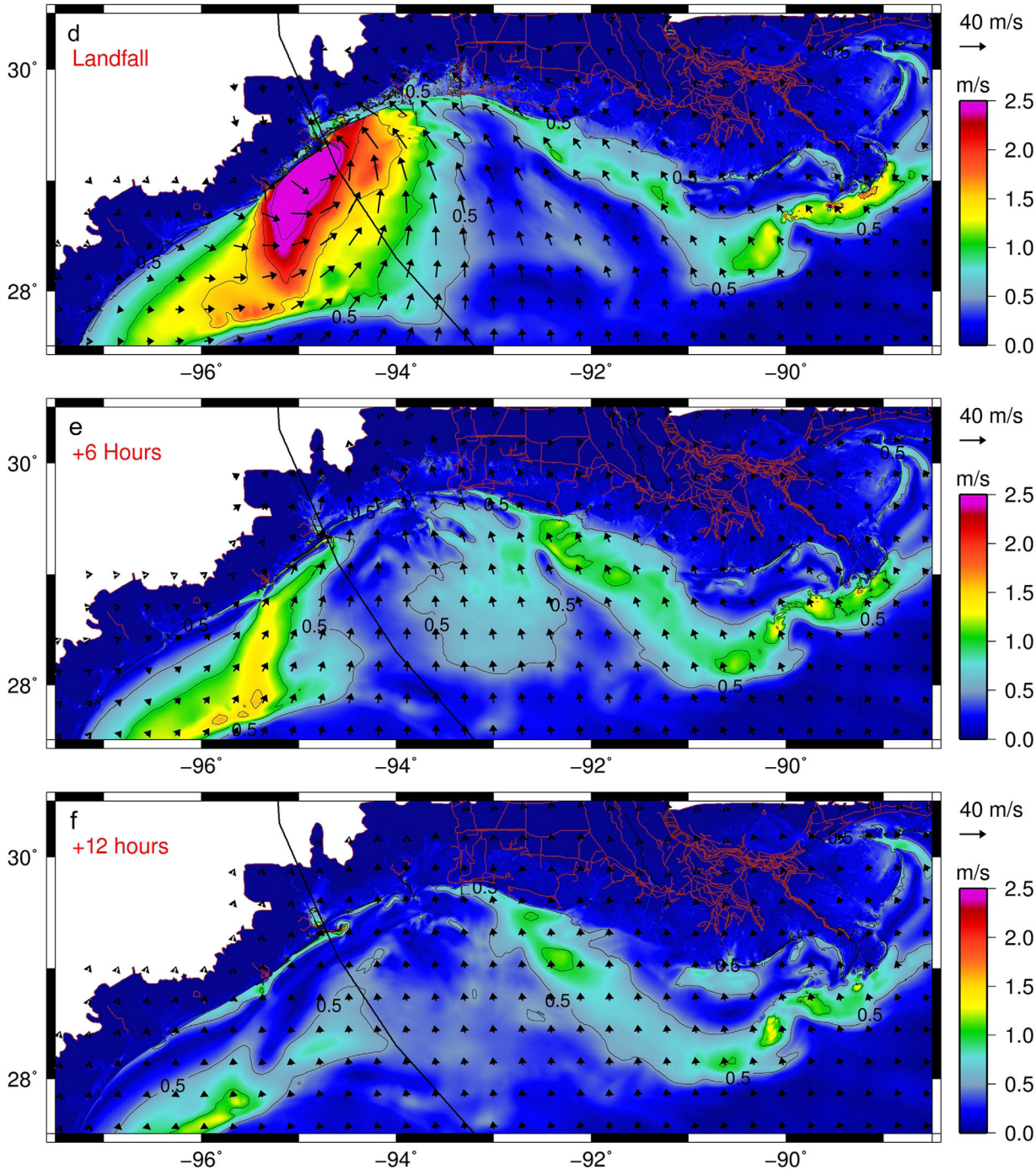

Figure 8. (continued)

on the timing of the maximum significant wave height and peak period at the time of maximum significant wave height (Figure 17), the largest waves at stations V, S, and R were the result of swell generated offshore.

[42] SWAN, WAM, and STWAVE wave characteristics are compared to measured values at representative stations in Figures 12–17. At the deep water, NDBC buoys 42039, 42036, 42001, 42002, and 42055 are shown in Figures 12–15, both SWAN and WAM capture the growth of swell waves as Ike progresses through the Gulf. At nearshore buoys, SWAN more accurately captures the maximum significant wave heights, as seen at NDBC buoy 42007 near the Mississippi-Louisiana coast (Figures 12 and 13). At NDBC buoy 42002, a dramatic departure is seen between the recorded and computed mean wave direction and the mean wave direction modeled by SWAN beginning at landfall. This is due to the measurement range limitation of high wave frequencies at NDBC buoys due to the nature of these large wave gages. By landfall at buoy 42002, the sea state had transitioned to locally generated wind waves, which are not accurately captured by the large NDBC buoys. Therefore, the mean wave direction is based on the

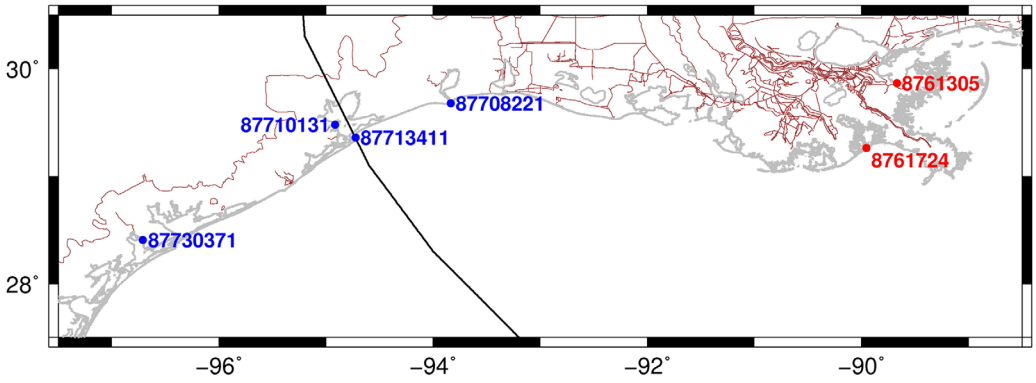

Figure 9. Locations of NOAA and TCOON stations on the LATEX shelf. NOAA in red, TCOON in blue. Ike track is in black, the coastline is in gray, and SL18TX33 boundary and raised features in brown.

dominant wave period that can be captured by the buoy, which in this case does not align with the local wind waves.

[43] In the Biloxi Marsh, SWAN captures the small, locally generated waves as seen at stations USACE CHL 2410510B, 2410523B, and 2410504B (Figures 16 and 17). At the CSI gages 05 and 06 south of Terrebonne Bay, SWAN accurately captures the arrival of swell generated offshore (Figures 16 and 17). North of Terrebonne Bay at CHL gage 2410512B, SWAN accurately models the small 1 m significant wave height, but slightly overestimates the peak wave period of 3 s (Figures 12, 16, and 17). As in the Biloxi Marsh, wave solutions in this area are highly sensitive to water depth and bottom friction.

[44] On the outer TX shelf at NDBC buoys 42020 and 42019, both SWAN and WAM capture the development of swell and peak significant wave heights. At nearshore NDBC buoy 42035, WAM severely underpredicts the development of swell and peak significant wave height, whereas SWAN captures the peak as well as wave growth (Figures 12–14). At AK's inner shelf gages along the TX coast, both SWAN and STWAVE capture maximum significant wave heights as well as wave growth prior to landfall (Figure 16). At AK stations X, Y, and Z, peak significant wave heights were wind-seas generated by strong landfalling winds. This is opposed to stations V, S, and R where winds were weaker and maximum wave heights were generated by swell in the deep Gulf. Figure 16 shows a late arrival of the peak significant wave height at AK stations X, V, S, and R. This late arrival of maximum significant wave heights at the inner shelf stations away from landfall, and underprediction of waves prior to landfall at stations near Ike's landfall location, indicates an artificial retardation of swell across the TX shelf. Despite this, SWAN models the quick transition from swell to wind-sea at landfall, as shown in Figure 17. STWAVE also captures this transition, but it is more gradual in comparison to SWAN.

[45] For all measured time series, agreement of modeled results to measured data can be quantified via the Scatter Index (SI):

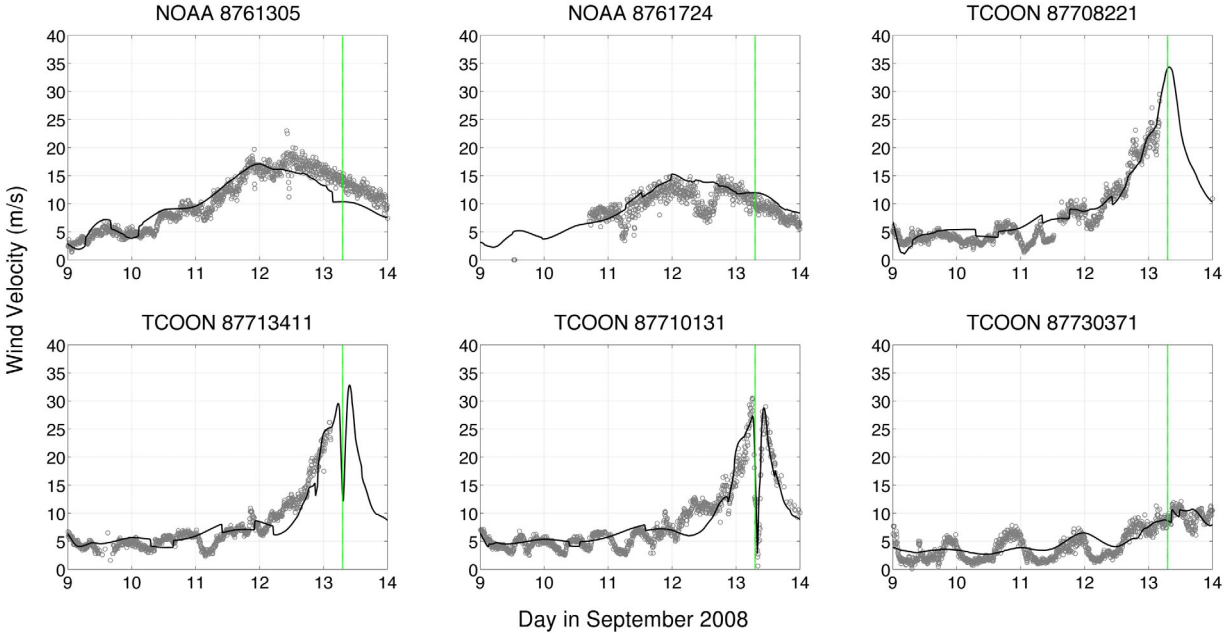

Figure 10. Time series (UTC) of wind velocities (m s^{-1}) at NOAA and TCOON stations. ADCIRC output in black, Observation data in gray. Dashed green line represents landfall time.

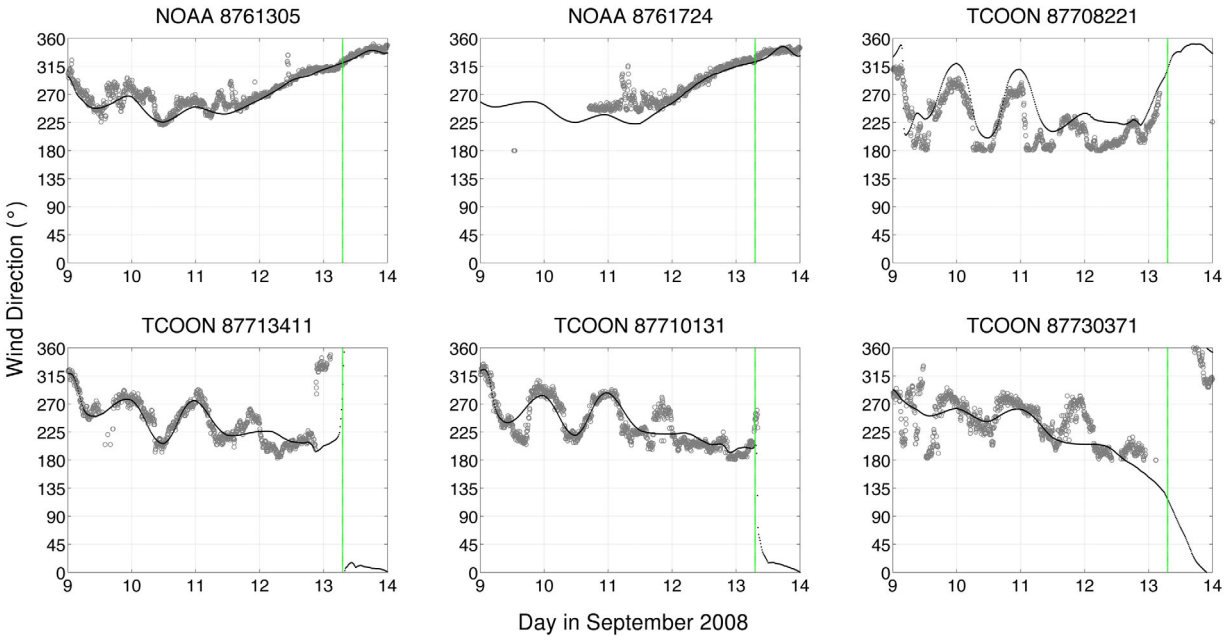

Figure 11. Time series (UTC) of wind direction (°) at NOAA and TCOON stations. ADCIRC output in black, observation data in gray. Dashed green line represents landfall time.

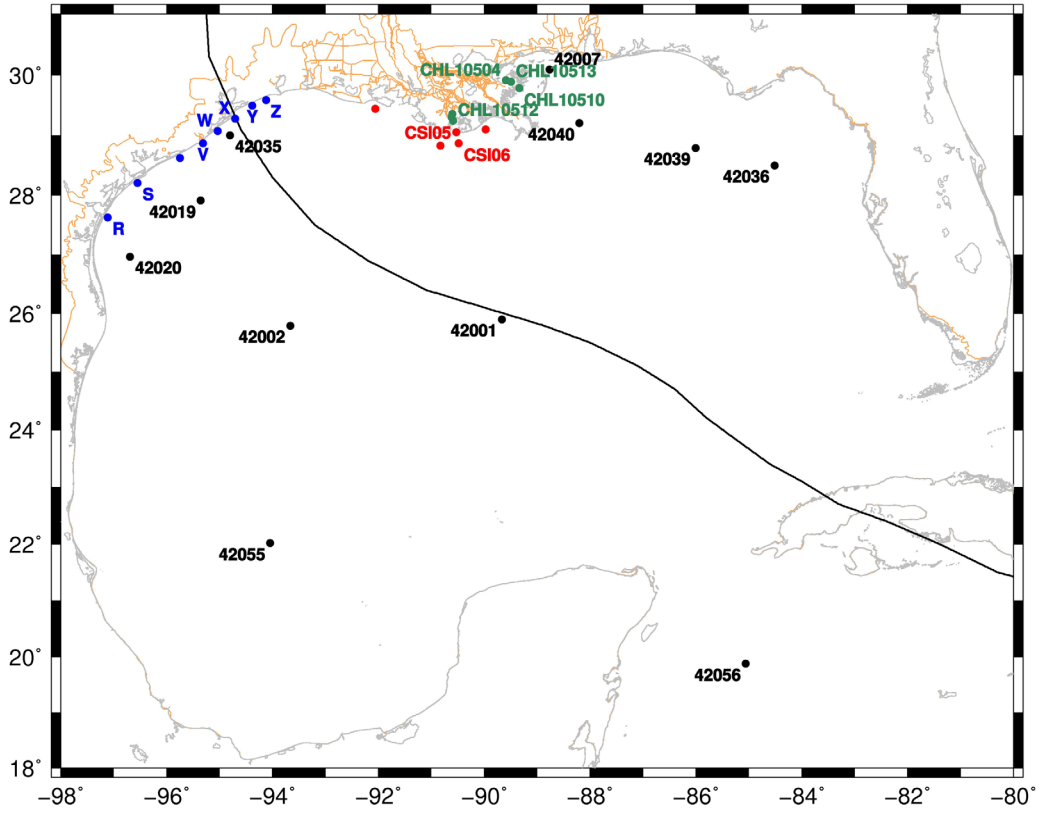

Figure 12. Locations of NDBC, CSI, CHL, and AK gages in the Gulf of Mexico. NDBC in black, CSI in red, CHL in green, and AK in blue. Ike track is in black, the coastline is in gray, and SL18TX33 boundary and raised features in brown. NDBC 42058 lies outside the frame in the Caribbean Sea.

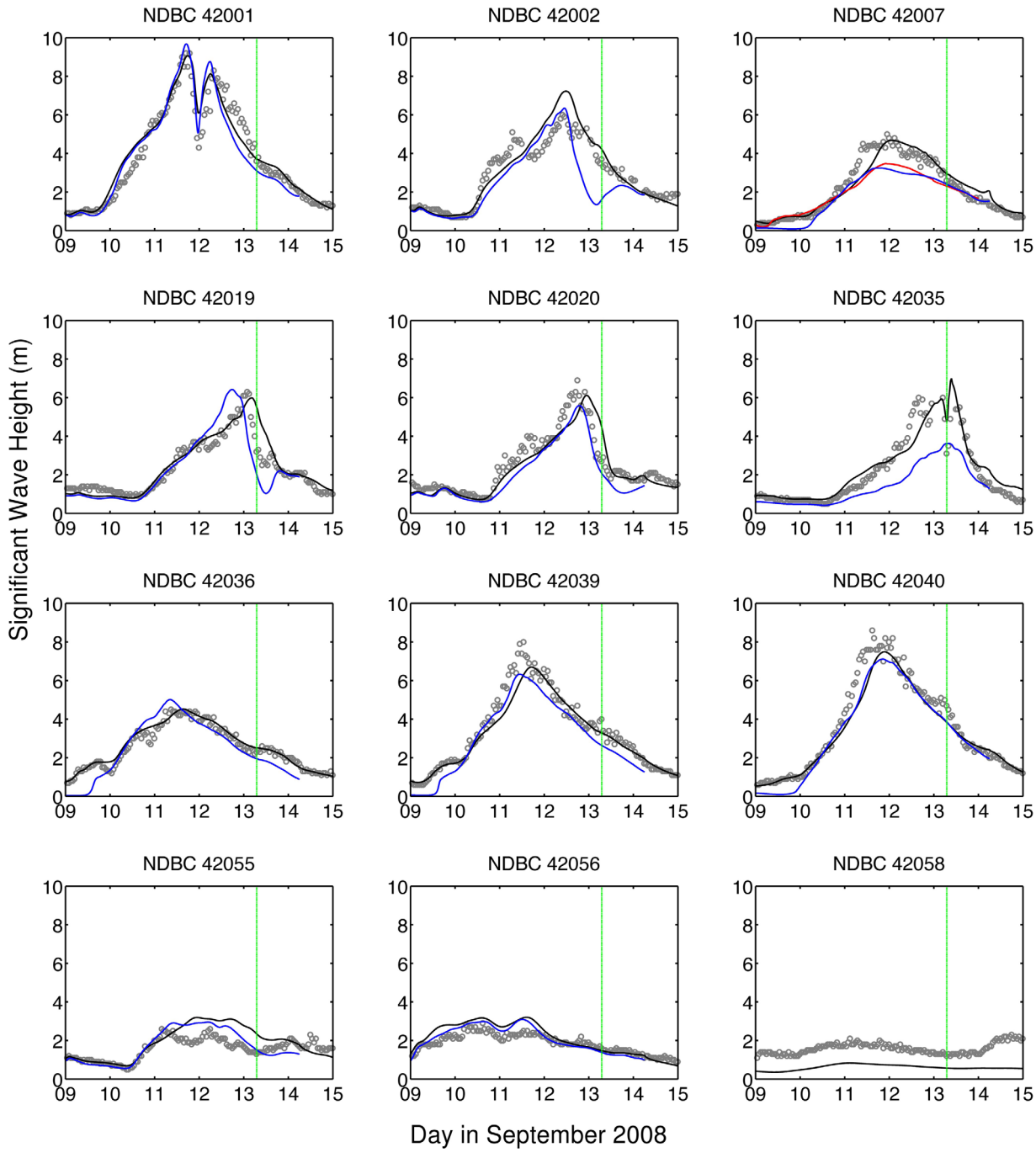

Figure 13. Time series (UTC) of significant wave heights (m) at 12 NDBC stations. SWAN results are in black, WAM results are in blue, and STWAVE results are in red. Dashed green line represents landfall time.

$$SI = \frac{\sqrt{\frac{1}{N}\sum_{i=1}^{N}\left(E_i - \overline{E}\right)^2}}{\frac{1}{N}\sum_{i=1}^{N}|O_i|}$$

and normalized bias:

$$bias = \frac{\frac{1}{N}\sum_{i=1}^{N}E_i}{\frac{1}{N}\sum_{i=1}^{N}|O_i|}$$

where N is the number of observed data points, S_i is the modeled data value, O_i is the measured value, $E_i = S_i - O_i$, and $\overline{E}$ is the mean error [*Hanson et al.*, 2009]. The SI is the ratio of the standard deviation of model error to the mean measured value. Tables 4 and 5 summarize SI and bias for all measured wave data. It should be noted that WAM and STWAVE are subject to slightly different wind forcing than SWAN. SWAN receives its winds from ADCIRC where overland winds are reduced due to directional onshore roughness. Thus, a narrow zone of offshore

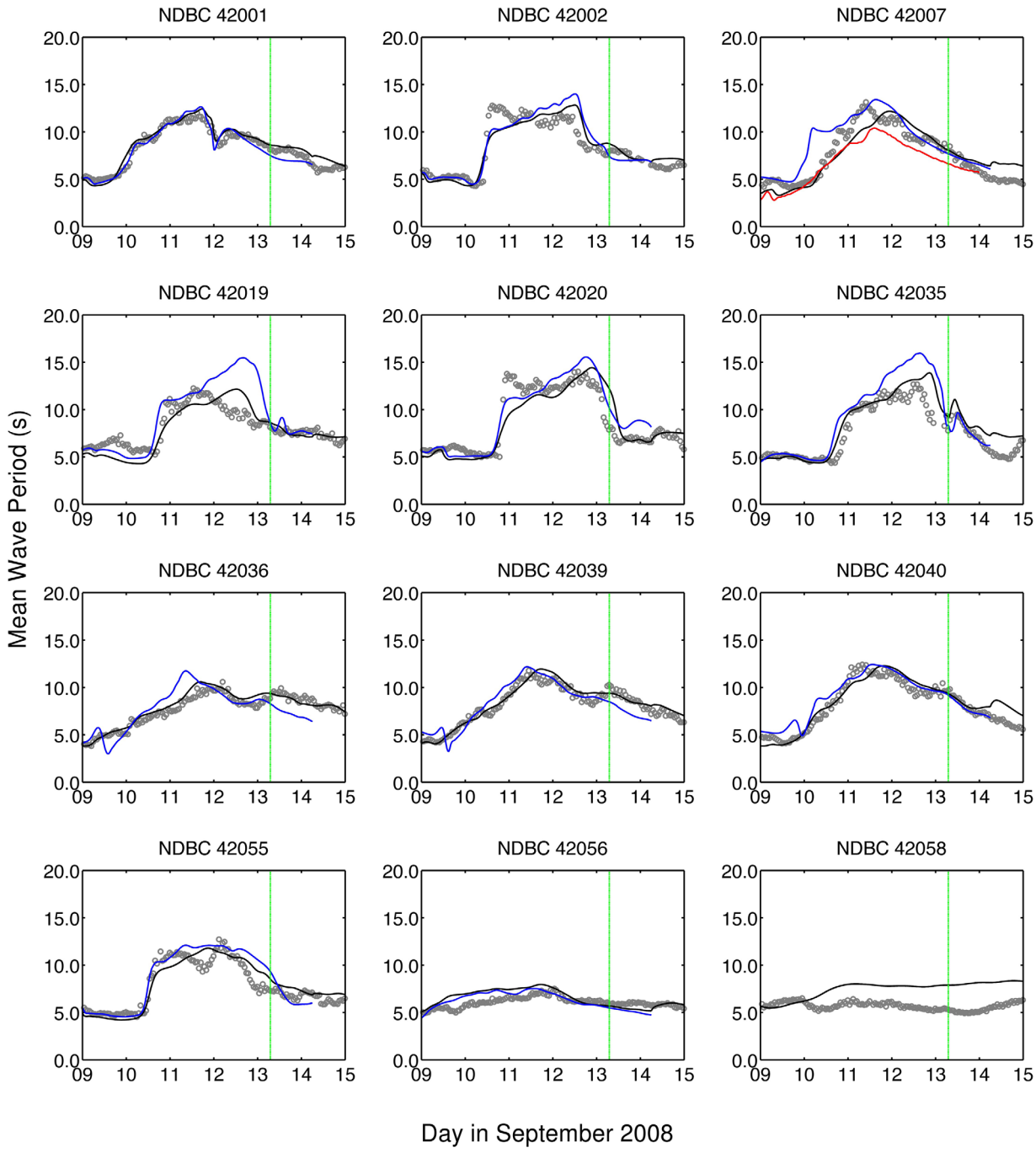

Figure 14. Time series (UTC) of mean wave period (s) at 12 NDBC stations. SWAN results are in black, WAM results are in blue, and STWAVE results are in red. Dashed green line represents landfall time.

directed winds adjacent to noninundated land areas will be different. However, the offshore marine winds with no land boundary layer adjustments are the same for all three models.

[46] Table 4 summarizes model performance at every station within each wave model's domain, while Table 5 summarizes error statistics only at stations shared by at least two wave models. In general, good agreement is seen between SWAN and WAM/STWAVE to measured data at NDBC, CSI, and AK gages. SI and bias values for significant wave heights, mean and peak periods, and mean direction at NDBC, CSI, and AK gages are similar to those found in previous SWAN + ADCIRC validation studies [*Dietrich et al.*, 2011a]. Table 4 provides an overall assessment of model performance, but to understand how the wave models performed in relation to one another, Table 5 must be examined. Overall, SWAN and WAM/STWAVE perform comparably, but some regional and model differences can be discerned by looking at model performance in differing coastal geographies at common stations. At

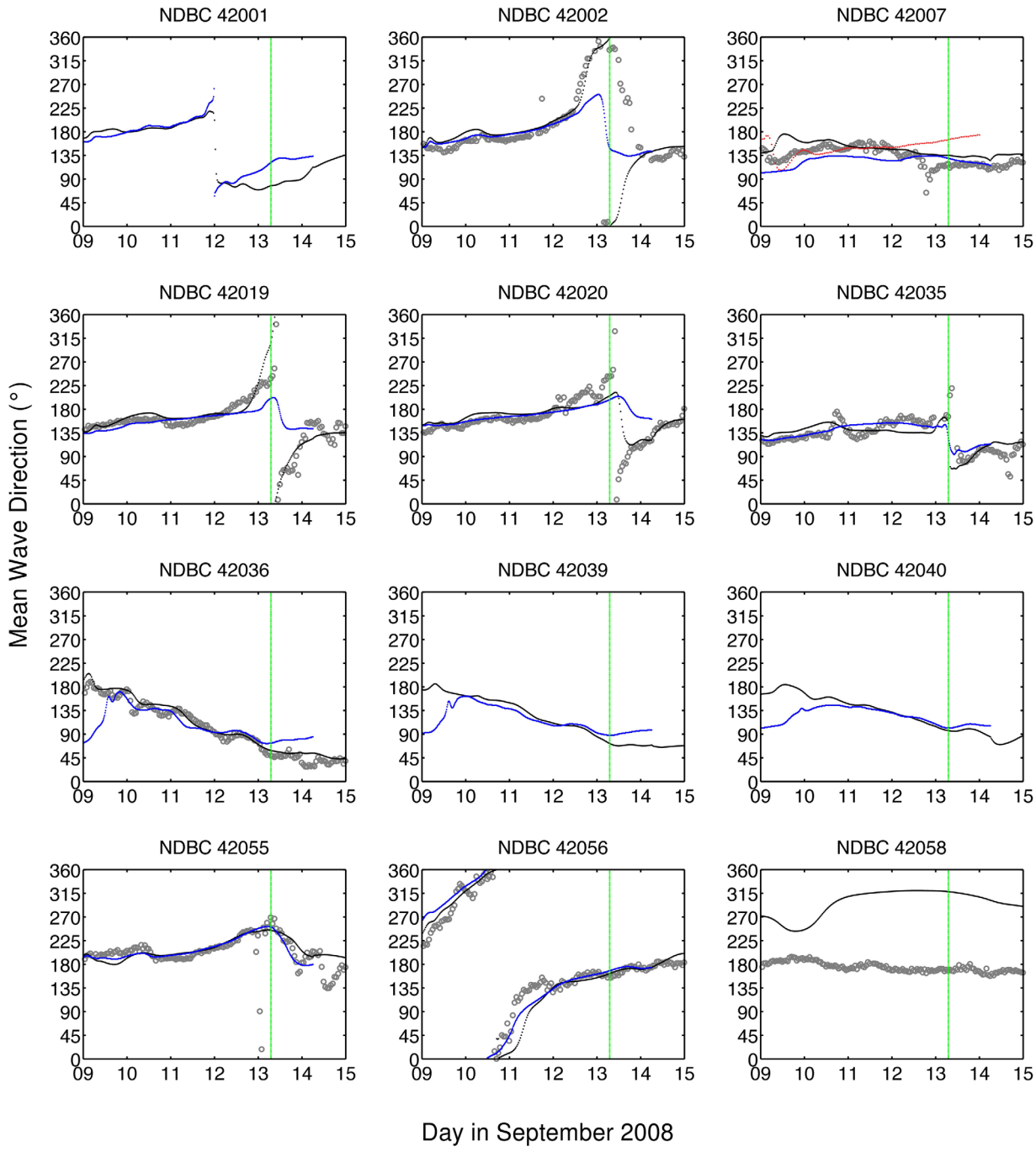

Figure 15. Time series (UTC) of mean wave direction (°) at 12 NDBC stations. SWAN results are in black, WAM results are in blue, and STWAVE results are in red. Dashed green line represents landfall time.

stations common to both SWAN and WAM/STWAVE, wave heights are overestimated for all geographic locations and models with the exception of WAM/STWAVE at NDBC buoys. SI and bias increase as stations are located in increasingly shallow water implying a trend of overestimated wave heights in very shallow water. A slight advantage is seen with WAM/STWAVE in peak wave period in coastal waters. For inland waters, SWAN performs better for peak period. It should be noted that wave heights are small at inland stations. Mean wave direction represents the wave parameter where one model clearly outperforms the other. SWAN has significantly lower bias and SI compared to WAM/STWAVE in deep water. Unfortunately, mean wave direction was only recorded at NDBC deep water stations, making it impossible to see if the spatial trend of increasing accuracy in deep waters extends to shallower water. The spatial trend of decreasing accuracy and differing model results in shallow water may be due to each model's representation of bathymetry, mesh resolution, and the general increased sensitivity of wave

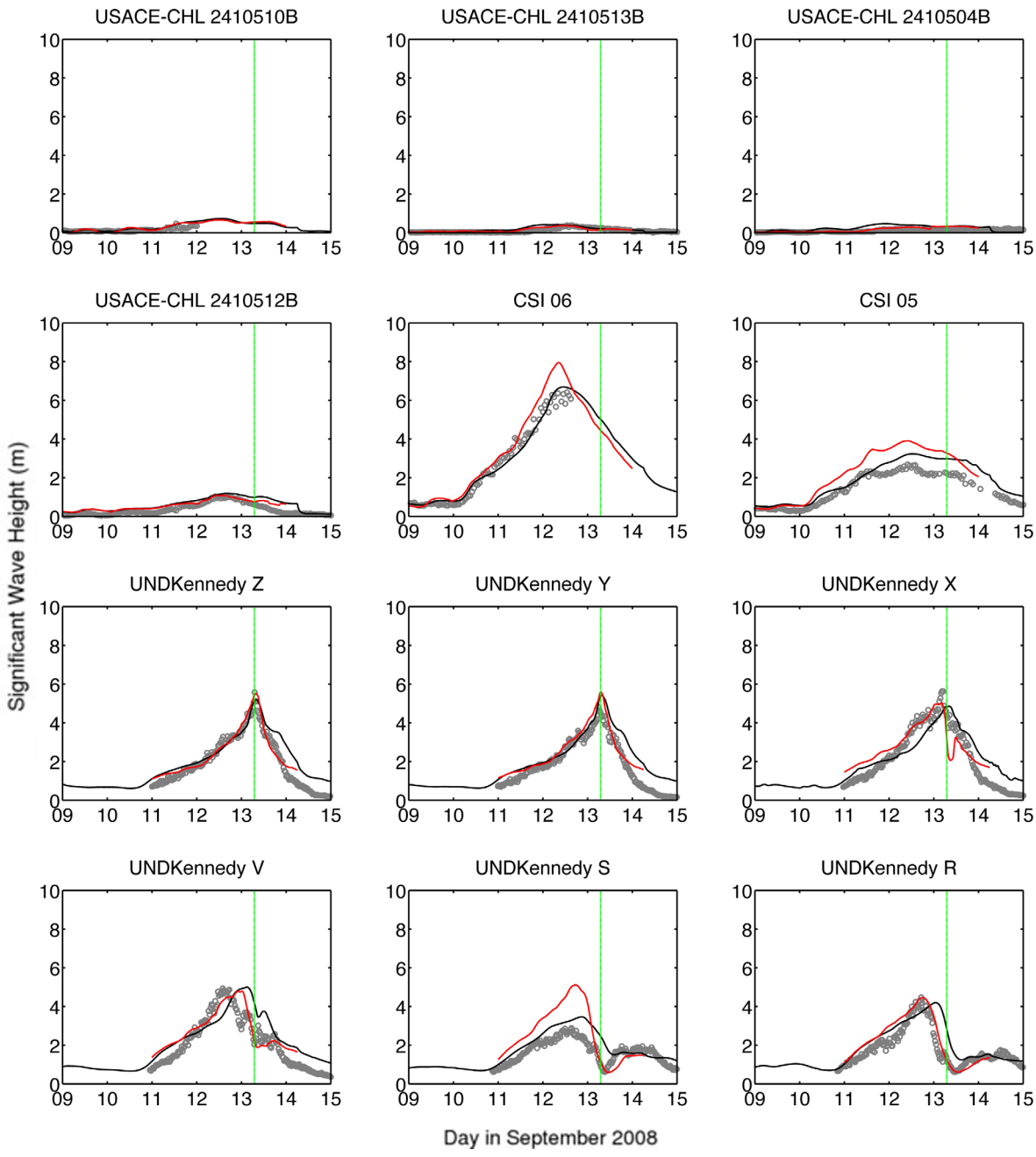

Figure 16. Time series (UTC) of significant wave heights (m) at 12 CSI, CHL, and AK gages. SWAN results are in black and STWAVE results are in red. Dashed green line represents landfall time.

parameters to shallower depths. WAM, STWAVE, and SWAN operate on different grids with very different levels of grid resolution in the nearshore affecting process resolution and the depiction of bathymetry in the various models. This is likely the cause of some of the differences in the solutions of the models at NDBC station 42007 and 42035. Specifically, the WAM grid is poorly resolved at these stations where large gradients in bathymetry and wave characteristics occur. Particular attention must be given to the inland gages where both SWAN and WAM/STWAVE performed poorly in proportionally based errors due to the small wave amplitude values. The inland sample size is small (4 gages), but the poor results indicate a deficiency in modeling waves in shallow inland waters. This deficiency stems from the large sensitivity of small inland waves to water levels and bottom friction parameterization. The fact that both models produce poor results and the water surface elevation results produced by ADCIRC, which are used to force the wave models, are quite accurate (Table 6), would indicate that both the SWAN and WAM/STWAVE models suffer from poor bottom friction parameterization for short, inland wind waves.

4.3. Surge and Currents

[47] Ike's unusually large wind field in the Gulf of Mexico resulted in a myriad of surge processes occurring over a

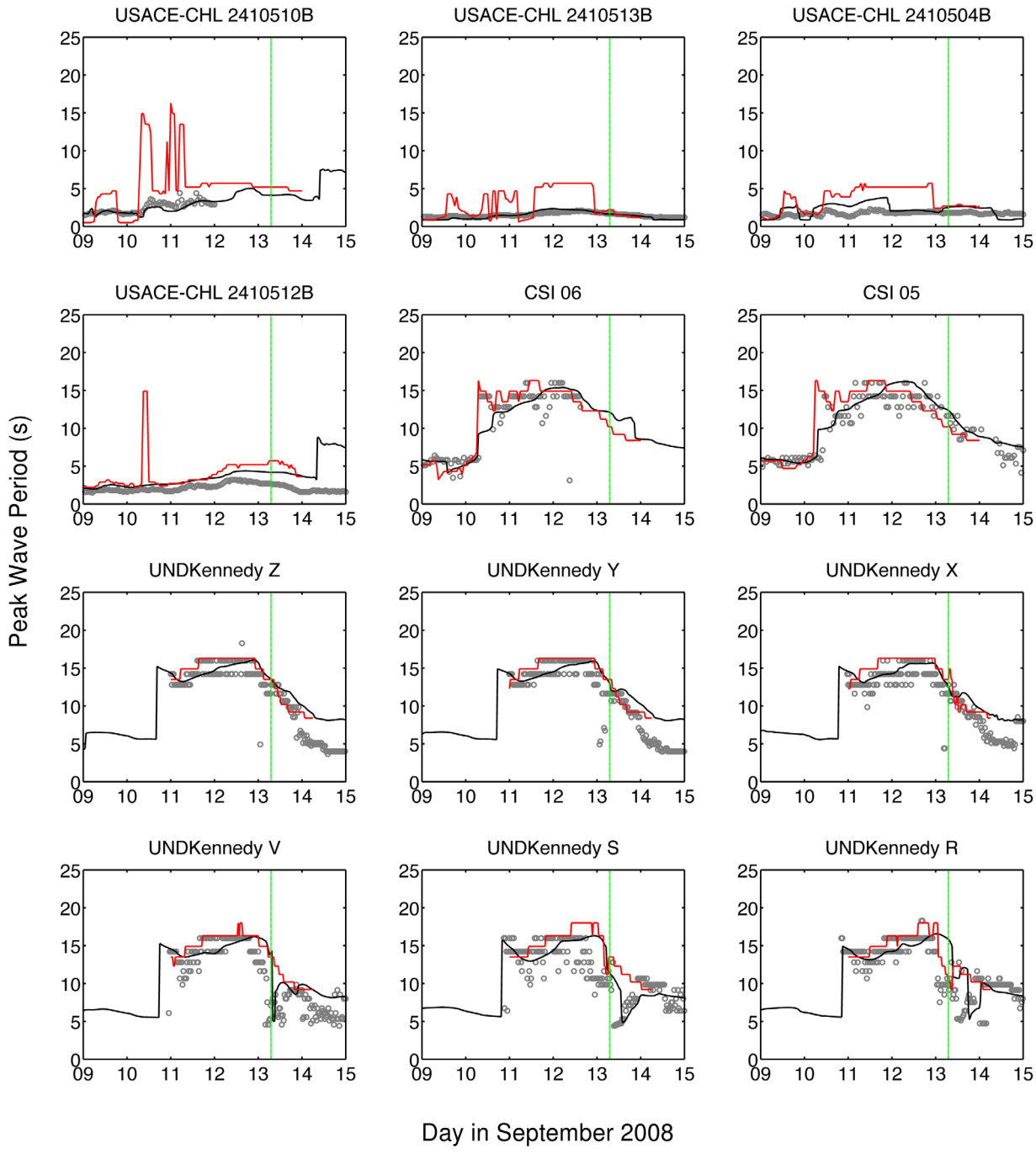

Figure 17. Time series (UTC) of peak wave period (s) at 12 CSI, CHL, and AK gages. SWAN results are in black and STWAVE results are in red. Dashed green line represents landfall time.

1000 km stretch of the LATEX shelf and coast. The storm surge response is regional and depends on the geography and orientation of the shelf and the characteristics of the storm.

[48] Due to Ike's large wind field and track across the Gulf of Mexico, easterly winds persisted over the Mississippi, Chandeleur, and Breton Sounds for over 36 h. While the winds over these Sounds never exceeded 20 m s^{-1}, the long duration and steady direction allowed for effective penetration of surge generated over these waters and into the lakes and marshes surrounding New Orleans (Figure 7). NOAA gages 8761305 and 8761927 (Figures 18 and 19) located on the south shore of Lakes Borgne and Pontchartrain recorded a maximum surge level of 2.1 m and 1.8 m, respectively, 15 and 7 h before landfall. The similarity in these hydrographs (with a time lag as the water moves inland) demonstrate the large-scale spatial response in the region and the slow time scale of the response allowing Lake Pontchartrain to be effectively filled. To the southeast of New Orleans, winds over the Chandeleur and Breton Sounds forced surge into the Biloxi and Caernarvon Marshes to the east of the Mississippi River and against the

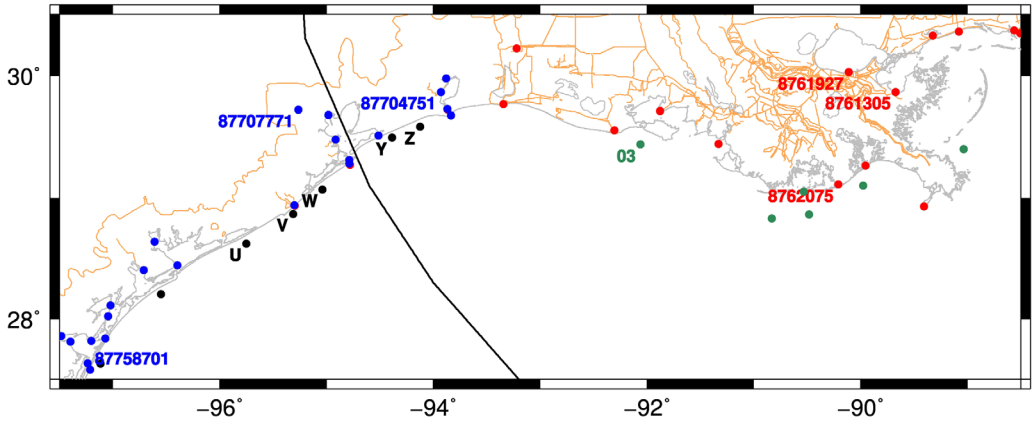

Figure 18. Locations of AK, NOAA, TCOON, and CSI gages on the Louisiana-Texas coast. AK in black, NOAA in red, TCOON in blue, and CSI in green. Coastline is in gray and SL18TX33 boundary and raised features in brown.

associated levee systems. The Delta and levee system extends far onto the continental shelf, effectively capturing the locally generated surge coming from the shallow waters to the east of the Mississippi River. CHL gages 2410504B and 2410513B and CRMS gage CRMS0146-H01 (Figures 20 and 21), located in the Biloxi and Caernarvon Marshes, all recorded maximum surge levels of 2 m. Water levels rise as the surge is blown over the shallow Caernarvon marsh and against the river levee south of English Turn in Plaquemines Parish where surge reached 3 m, indicating that no attenuation in surge occurred over the Caernarvon Marsh. In fact, the steady winds allowed water levels to increase across the marsh.

[49] The buildup of surge to the east of the Mississippi River, combined with the lack of surge buildup to the west of the river created a water surface gradient that produced a strong current around the Delta (Figure 8). This 2 m s^{-1} current persisted to the south of the Delta for over 24 h.

[50] To the west of the Delta, the narrow continental shelf allowed large swell generated in the deep Gulf to propagate close to coastal wetlands. The coast in this area experienced slightly onshore, moderate velocity (not exceeding 20 m s^{-1}) winds, and when combined with the wave setup caused by large breaking waves nearshore, a slow rise of water was observed. Simulations where the wave interaction was neglected indicated that up to 50% of storm surge on the Delta was generated by wave setup. This is consistent with the steep bathymetry in the region and previously validated storms [*Dietrich et al*., 2011a, 2010; *Bunya et al*., 2010; *Kerr et al*., 2013a, 2013b]. USACE gage 82260 and USGS-Perm gage 292800090060000 (Figures 20 and 21), located in this region to the northwest of Barataria Bay, recorded maximum water levels of 2 m and 1.6 m, respectively.

[51] To the west of Barataria Bay, the continental shelf progressively broadens to over 200 km at its widest point in the vicinity of Lakes Sabine and Calcasieu. This wide, shallow shelf and large scale concave coastal geography of the LATEX coast combined with Ike's steady prelandfall winds to generate a strong, long-lasting, shore-parallel current (Figure 8). Figure 23 shows the location of observed currents on the LATEX shelf and Figures 24 and 25 show ADCIRC and observed current velocity and direction. On the Louisiana shelf, CSI station 3 shows a gradual increase in current speed beginning on 12 September, reaching its recording maximum value of 1 m s^{-1} 12 h before landfall. On the Texas shelf (Figures 23–25) at the Texas Automated Buoy System (TABS), current data buoys show the development of the forerunner driving current. Unfortunately, the TABS buoys are not able to record currents in excess of 1 m s^{-1} as is seen in the plateau in the velocities. As the storm approached, the steady, shore-parallel current created a geostrophic setup that caused a rise in water at the coast starting 24 h before landfall [*Kennedy et al*., 2011a, 2011b]. This geostrophic setup, typically identified as a forerunner surge, is only possible due to the strong (more than 1 m s^{-1}) shore parallel current driven by shore parallel winds as seen in Figures 4, 8, 10, and 24. The low bottom friction and wide shelf are vital components to the large amplitude of the forerunner. Figure 7a shows 1 m of surge has developed on the entire LATEX shelf 18 h before landfall, when winds on the coast did not exceed 20 m s^{-1} and were generally shore parallel or directed offshore. This geostrophic setup is illustrated at several gages across the LATEX coast. UND Kennedy Z and Y (Figure 19) both show a gradual rise in water beginning early on 12 September 2008, 24 h before landfall. Similar to the flooding process to the east of the Mississippi River, the long time scale of the geostrophic process allowed water to penetrate far inland. Onshore in Texas, TCOON gages 87704751 and 87707771 (Figures 18 and 19), located inland in Lake Sabine and Galveston Bay, respectively, both recorded a rise in water starting early on 12 September 2008, when winds at the coast were still strongly shore-parallel or slightly offshore. These two TCOON gages are of particular interest because they demonstrate the inland penetration of the forerunner surge into coastal lakes and bays in advance of landfall. This early inundation only weakly affects peak surge at the coast because the forerunner surge propagated down the LATEX shelf prior to the landfall of the storm and the primary surge in open water is generated by land-falling shore perpendicular winds. However, the forerunner is critical to inland coastal estuarine and wetland areas, particularly regions that would later experience the strong winds associated with landfall. The early penetration

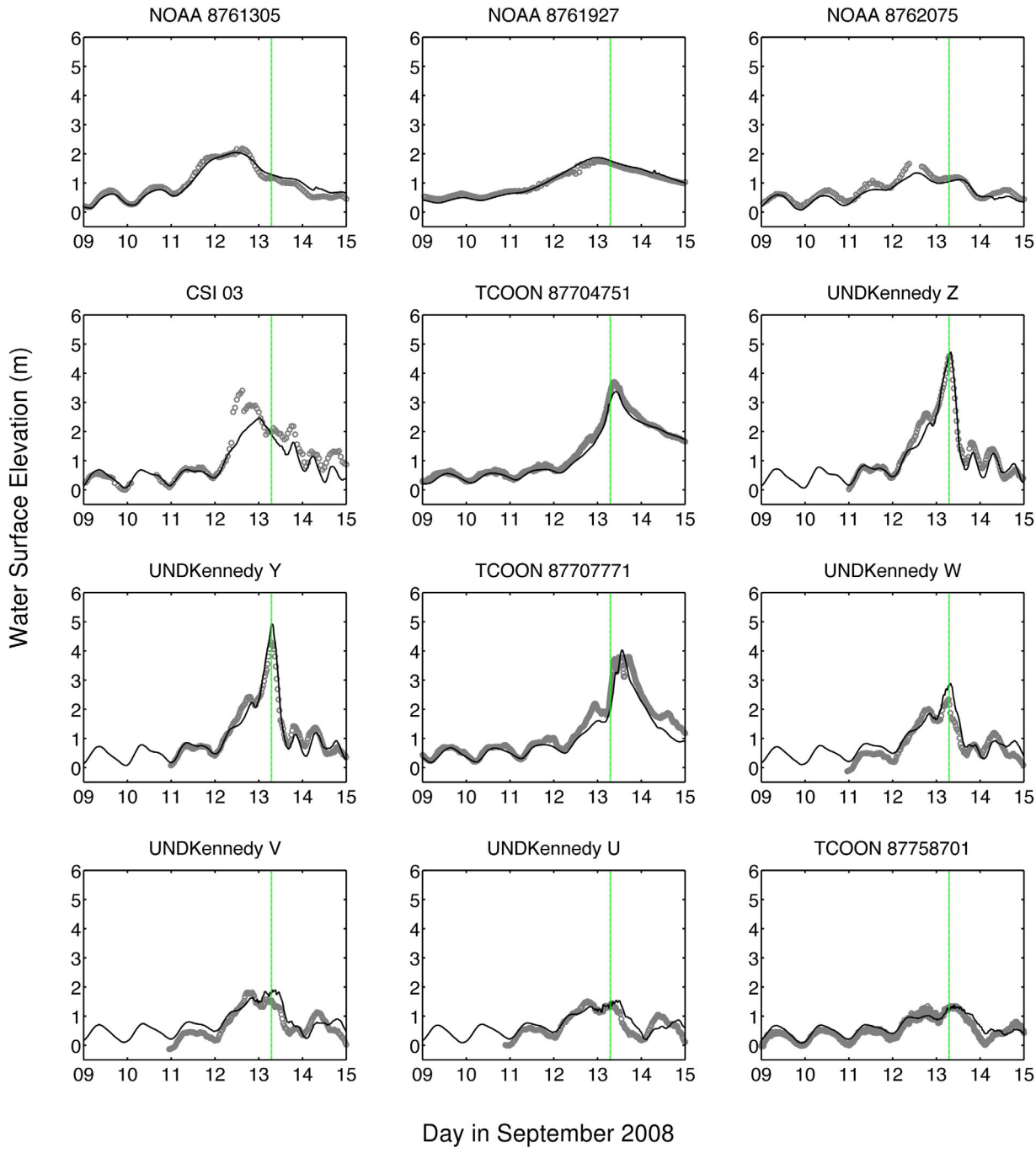

Figure 19. Time series (UTC) of water surface elevations (m) at 12 AK, NOAA, TCOON, and CSI gages. ADCIRC output in black, observation data in gray. Dashed green line represents landfall time.

occurs at a slow time scale and is retained by the inland waters after the propagation of the open water forerunner down the shelf toward Corpus Christi. This early inland inundation and retention exacerbated the impact of the locally generated surge within inland coastal lakes and bays at landfall.

[52] Following generation, the geostrophically driven forerunner surge propagated down the shelf as a free continental shelf wave. To the southwest of landfall, the forerunner surge can be seen in Figures 7d–7f and 8a–8f. Propagating down the shelf, the peak of the free wave reached Corpus Christi and TCOON gage 87758701 (Figures 18 and 19) as Ike was making landfall on the Bolivar Peninsula.

[53] Prior to landfall (Figures 7a–7c), water levels in the region near landfall are driven by a predominantly shore-parallel process: the forerunner surge. Starting in Figure 7d, surge at the coast of the Bolivar Peninsula has transitioned to a shore-normal process driven by strong shore-normal winds. Figure 7d shows the buildup of water against the Bolivar Peninsula and Figure 7e shows the wind-driven progression of water over the Peninsula inland and onto the coastal floodplain while the surge at the coast has rapidly

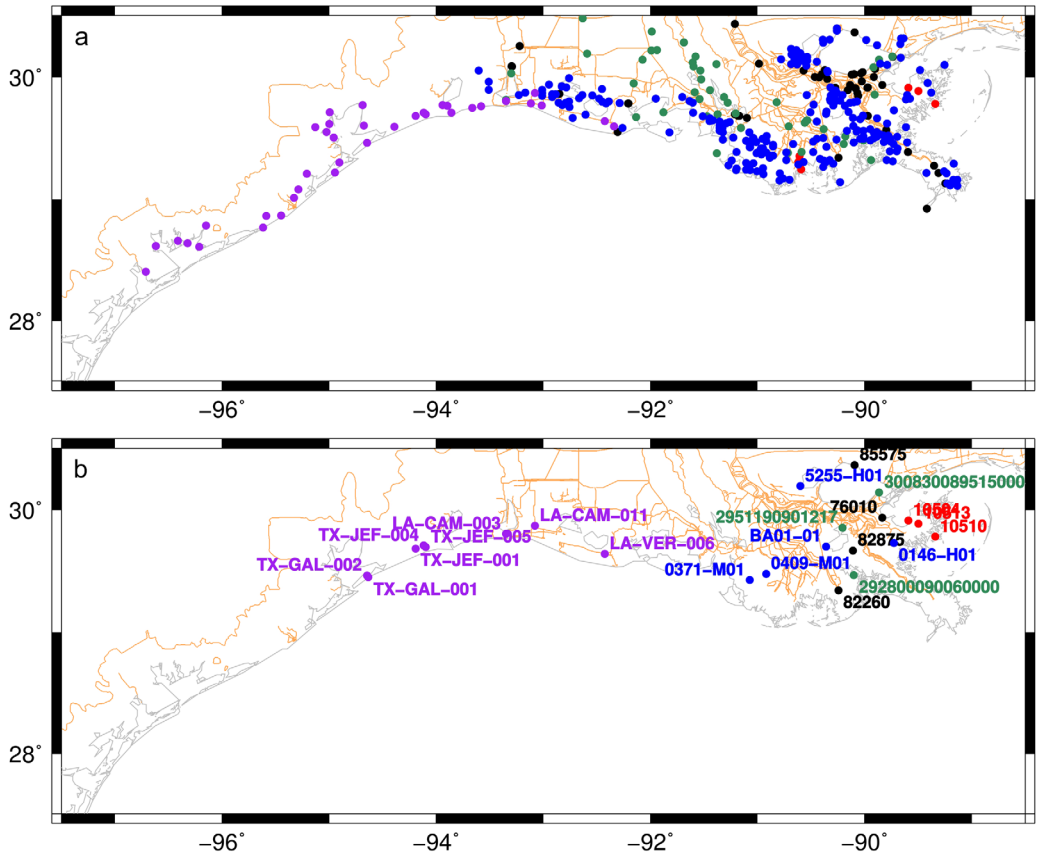

Figure 20. (a) Locations of USACE (black), USACE-CHL (red), USGS (green), CRMS (blue), and USGS-DEPL (purple) gages on the LATEX coast, (b) subset of locations shown in Figure 20a for which hydrographs are shown. Coastline is in gray and SL18TX33 boundary and raised features in brown.

recessed back into open water. Figure 7f shows the overland recession process, which is impeded by the persistent but weakening shore normal winds following landfall and also by the frictionally dominated coastal floodplain. AK stations Z and Y are offshore from the Bolivar peninsula and recorded a peak surge of 4.6 m and 4.3 m, respectively (Figures 18 and 19). Onshore, FEMA high water marks and USGS-Temp gages extensively covered the area near landfall. USGS-DEPL gages USGS-DEPL_SSS-TX-GAL-001 and USGS-DEPL_SSS-TX-GAL-002 were located on the Gulf side and bay side of Bolivar Peninsula and recorded maximum water levels of 4.8 m and 4 m, respectively (Figures 20 and 22). This lower bayside elevation relates to bay and inland penetration time scale lag due to frictional resistance. Inland sides of barrier islands will typically lag behind the open coast side due to overland frictional resistance and other processes, such as wave radiation induced setup at the coast from large swell waves. To the northeast of landfall, a consistent water level of 5 m was measured by USGS-DEPL gages USGS-DEPL_SSS-TX-JEF-001, USGS-DEPL_SSS-TX-JEF-004, and USGS-DEPL_SSS-TX-JEF-005 (Figures 20 and 22). Further inland, FEMA measured two still-water high water marks exceeding 5.1 m in Jefferson County, over 15 km from the coast, representing the highest recorded surge elevation during the event.

[54] Water recessed rapidly back onto the shelf and into the deep ocean from the almost 4.8 m mound of water driven against the shore at landfall. This flux of water toward the deep Gulf was reflected back toward the coast as an out-of-phase wave due to the abrupt bathymetric change at the continental shelf break. This process can be seen across the LATEX coast between the Atchafalaya Basin and Galveston Island. This cross-shelf reflection can be seen in Louisiana at CSI gage 03 and in Texas at AK gages Z, Y, and W (Figures 18 and 19). This reflection almost certainly relates to the shelf resonance as the post-storm secondary, and tertiary peaks occur at approximately 12 h intervals during the reflections. According to *Sorensen* [2006], the length of an open resonant basin at the basic mode is computed as:

$$L = \frac{T\sqrt{gH}}{4}$$

where L is the length of the open basin, T is the resonant period, and H is the water column depth. Assuming an average depth on the shelf of 30 m, the resonant basin length is approximately 185 km. This is consistent with the width of the LATEX shelf along western Louisiana and eastern Texas, which varies between 160 and 220 km. The 12 h resonant period of the broad LATEX shelf is also evidenced by the strong amplification of semidiurnal tides on this shelf [*Mukai et al.*, 2002]. The fluctuating current fields in Figures 8d–8f represent the signature of the cross shelf resonance.

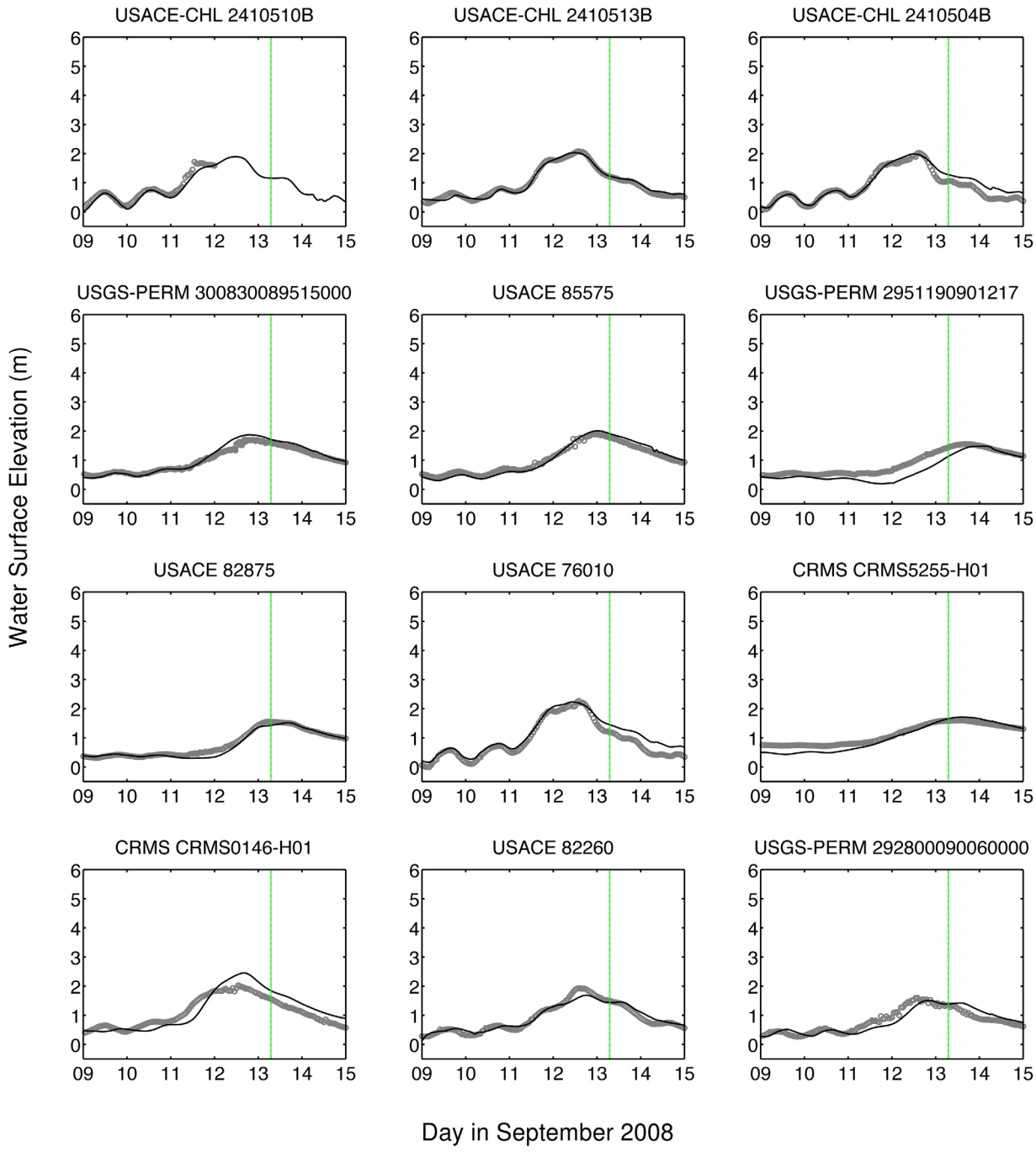

Figure 21. Time series (UTC) of water surface elevations (m) at 12 USACE, CHL, USGS, and CRMS gages. ADCIRC output in black, observation data in gray. Dashed green line represents landfall time.

[55] ADCIRC water surface elevations and currents are compared to measured values at representative stations in Figures 18–25. To the east of the Mississippi River, the ADCIRC model accurately captures the rise of water in the lakes and bays surrounding New Orleans, shown at NOAA gages 8761927 and 8761305 in Figures 18 and 19. The skill shown in modeling the surge generated on the Mississippi Sound that penetrated into Lakes Borgne and Pontchartrain indicates that the SL18TX33 model has adequate resolution in the small scale channels and passes hydraulically connecting the sound and lakes. In the Biloxi and Caernarvon marshes, the early rise in water and associated inland penetration process are captured by the model, shown at CHL gages 2410513B and 2410504B (Figures 20 and 21). ADCIRC slightly overpredicts the peak surge at CRMS gage CRMS_CRMS0146-H01 in the Caernarvon Marsh (Figures 20 and 21); however, based on the recorded data, it appears that the gage has an upper limit of measurement of 2 m. Model accuracy in this region indicates that the universally applied air-sea drag and bottom friction in marshes and wetlands in the region are correctly parameterized because the peaks are correctly captured and the flooding

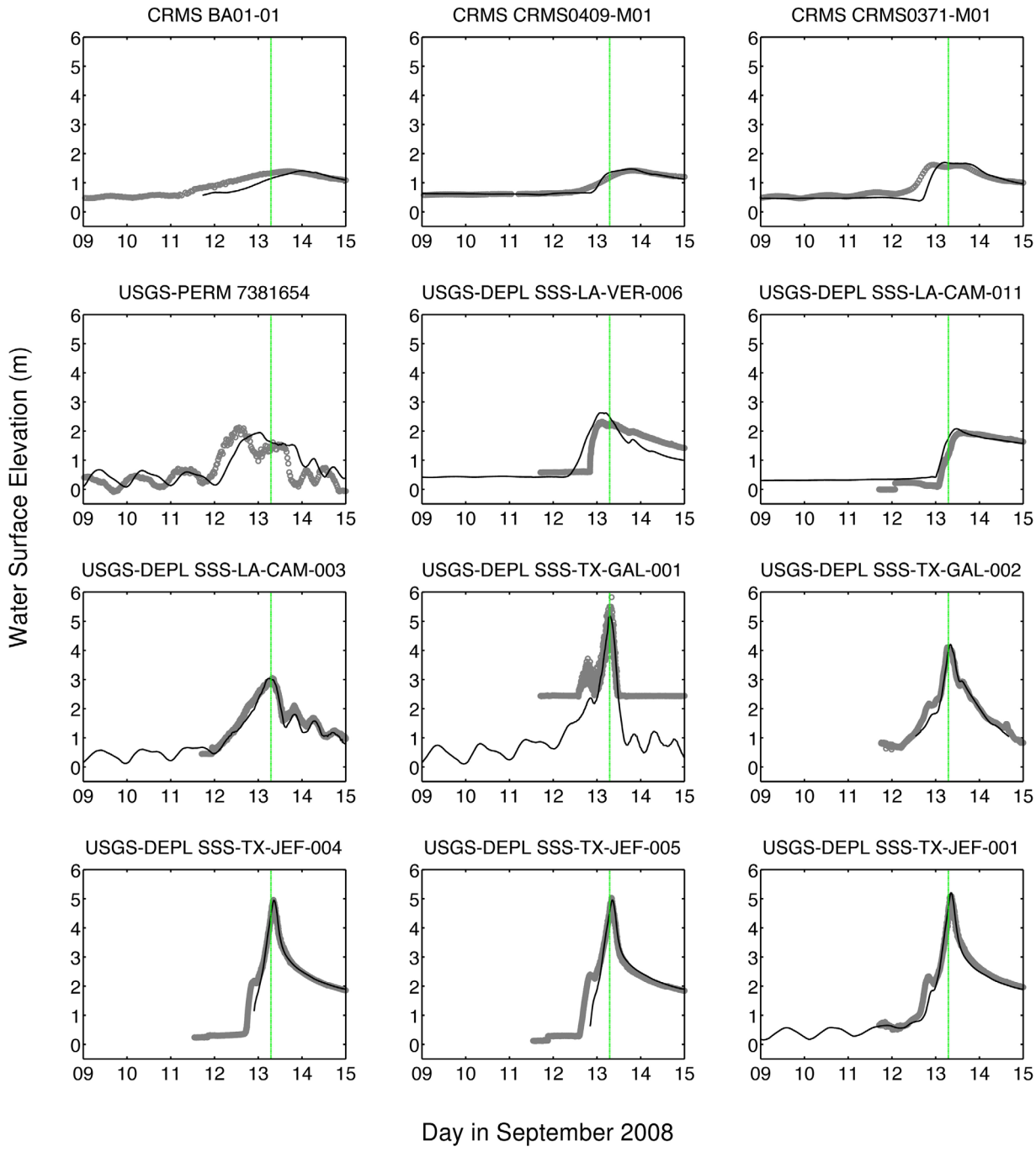

Figure 22. Time series (UTC) of water surface elevations (m) at 12 USACE, CHL, USGS, and CRMS gages. ADCIRC output in black, observation data in gray. Dashed green line represents landfall time.

and recession curves in this slow process are also well represented. During the recession of surge from the marshes, bottom friction is the controlling process in the shallow overland flow that occurs.

[56] To the west of the Delta, the complex interaction of large swell waves breaking nearshore, shore-normal winds, and a strong shore-parallel current is captured, with a slight underprediction of peak surge at USACE gage 82260 (Figures 20 and 21).

[57] The forerunner surge is a shelf scale process that is effectively captured by ADCIRC, as shown at gages USGS-PERM_07381654, USGS-DEPL_SSS-LA-VER-006, USGS-DEPL_SSS-LA-CAM-003, and USGS-DEPL_SSS-TX-GAL-002, AK gages Z, Y, W, V, and U, and TCOON gages 87704751 and 87707771 (Figures 18–20 and 22); but the modeled rise in water is slightly lower than the measured data at some gages. The model lag is most pronounced at gages AK Z and Y (Figures 18 and 19). This is also seen at TABS station B (Figures 23 and 24) where we note that between 3 and 15 h UTC on 12 September there is an underprediction in the shore parallel current speed by ADCIRC. This lag in forerunner surface elevations and the associated

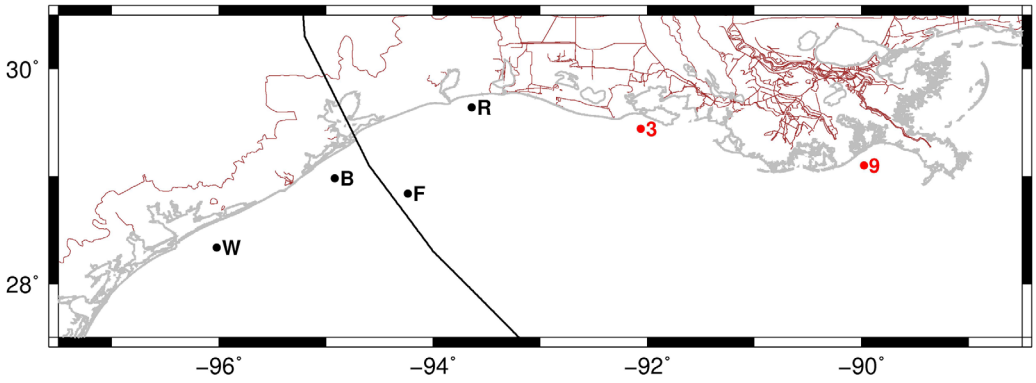

Figure 23. Locations of CSI and TABS stations on the Louisiana-Texas coast. TABS in black, CSI in red, coastline is gray, Hurricane Ike's track in black, and SL18TX33 boundary and raised features in brown.

currents is likely associated with the low bias in the OWI winds during this time in the region as seen at stations TCOON 87710131 and 87713411 (Figures 9 and 10). The forerunner surge process is reliant on the generation of the steady, strong shore-parallel current necessary for geostrophic setup. Due to the cap on the measured currents on the shelf at the CSI and TCOON gages, it cannot be determined if ADCIRC accurately modeled the peak currents, however, good agreement is seen between ADCIRC and observed velocities during most of the storm (Figures 23–25). ADCIRC also accurately captures the change in current direction as Ike moved across the shelf, with an exception at TABS B to the southwest of landfall where ADCIRC failed to model the quick change in direction that occurred right at landfall. Note that on the shelf, currents are likely quite uniform over depth due to the vigorous wave induced vertical mixing [*Mitchell et al*., 2005; *Sullivan et al*., 2012].

[58] The propagation of the free wave down the coast is captured by ADCIRC as seen at TCOON station 87758701 and AK stations V and U (Figures 18 and 19). In addition, the currents generated by the shelf wave are well represented in the model, as is shown by the comparisons at TABS station W (Figures 23–25).

[59] To the northeast of landfall, where the maximum surge levels occur, ADCIRC accurately models the peak shore normal wind-driven surge. ADCIRC shows good agreement to peak surge offshore at AK stations Z and Y, and inland at stations USGS-DEPL_SSS-TEX-JEF-005, USGS-DEPL_SSS-TEX-JEF-004, USGS-DEPL_SSS-TX-JEF-001, USGS-DEPL_SSS-TX-GAL-001, and USGS-DEPL_SSS-TX-GAL-002 (Figures 18–20 and 22).

[60] The 12 h resonant wave on the LATEX shelf resulting from coastal surge waters recessing into the deep Gulf is captured by ADCIRC. This is seen at water surface

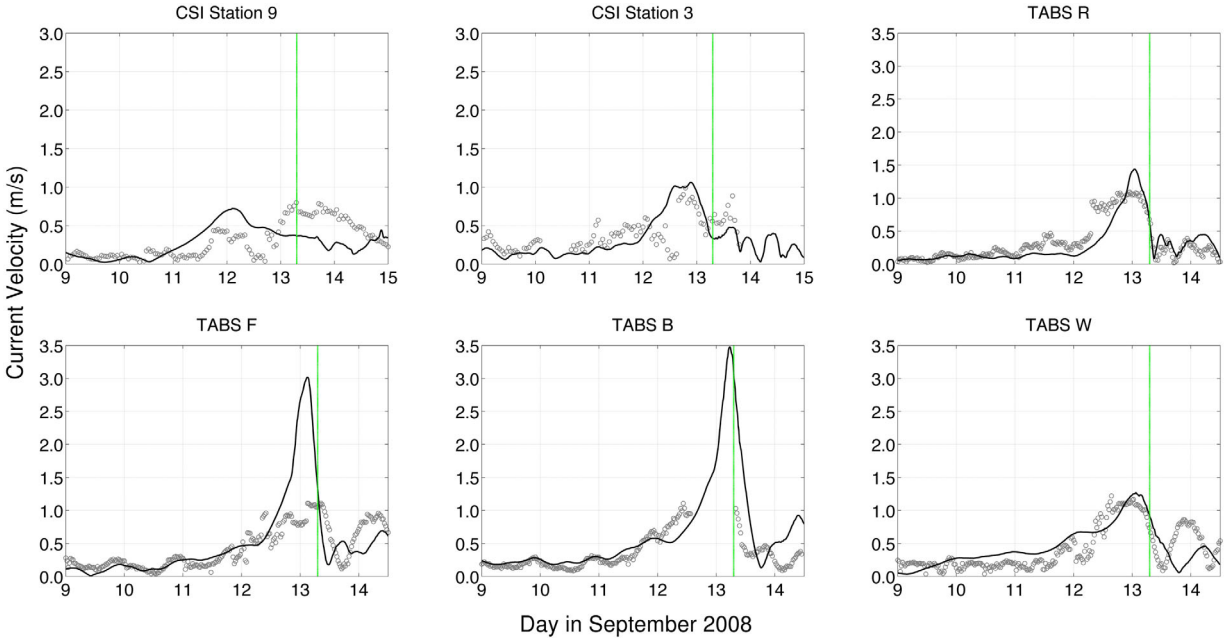

Figure 24. Time series (UTC) of current velocities (m s^{-1}) at CSI and TABS stations. ADCIRC output in black, observation data in gray, and dashed green line represents landfall time.

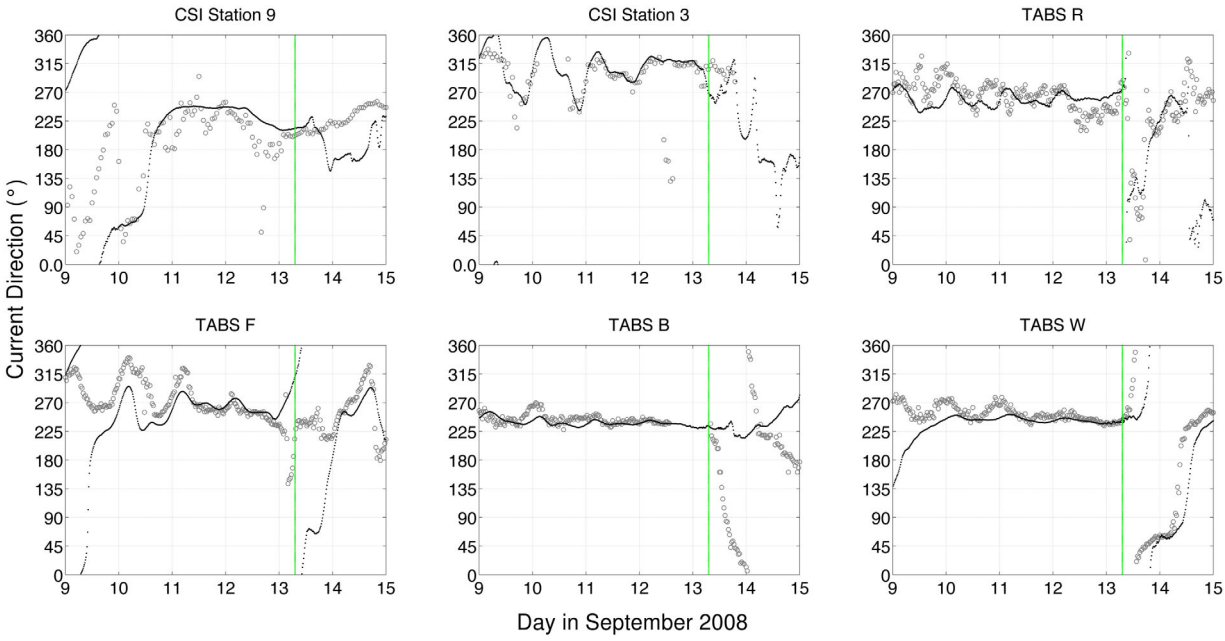

Figure 25. Time series (UTC) of current direction (°) at CSI and TABS stations. ADCIRC output in black, observation data in gray, and dashed green line represents landfall time.

elevations at AK stations Y and Z (Figures 18 and 19) and TABS current stations B and F (Figures 23–25).

[61] Maximum high water during the storm event is presented in Figure 26. A spatial analysis of differences between measured and modeled maximum high water at the 206 FEMA HWMs and at 393 hydrograph-derived high water values is shown in Figure 27. A comparison of model to measurement high water at these same 599 locations is shown in Figure 28.

[62] Table 6 summarizes the SI and bias of ADCIRC model results to recorded data for time series of water levels. The overall time series scatter index (SI) equals 0.1463 and indicates generally good agreement with the data. The bias of −0.0114 m indicates globally a small underprediction of water levels by ADCIRC. Examining both time series and HWM error statistics in Table 6 indicates that coastal stations are generally more accurately hindcast than inland stations. Coastal stations are slightly overpredicted while inland stations are slightly biased low. This is due to the general geographic simplicity, larger depths, and homogeneity of frictional resistance of the open coast as compared to the nearshore and especially floodplain. As hurricane-driven storm surge encroaches inland, any number of complexities including topography, bathymetry, heterogeneous frictional resistance, and subgrid scale impedances to flow can be found significantly complicating the flow. The poorest R^2 value is found at the CRMS stations (0.6833). The CRMS gages are located in Louisiana with the majority of stations located in inland marshes. Water levels in inland marshes are highly dependent on the level of connectivity to coastal water bodies and while the SL18TX33 mesh accurately represents major channels and connections, available bathymetric and topographic data is not of high enough resolution to properly represent all relevant connections.

Table 4. Summary of Scatter Index (SI) and Normalized Error Bias for Wave Data Time Series for All Data Stations in a Model's Geographic Coverage

		Sig. Wave Height			Peak Wave Period			Mean Wave Period			Mean Wave Direction		
Data Source	Model	Numberof Data Sets	SI	Bias	Number of Data Sets	SI	Bias	Number of Data Sets	SI	Bias	Number of Data Sets	SI	Bias
NDBC	WAM	10	0.1893	−0.0737	10	0.1571	0.0410	9	0.1248	0.0780	7	0.4379	0.7207
	STWAVE	1	0.1871	−0.1870	1	0.1271	0.0011	1	0.0812	−0.1463	1	0.1638	0.1348
	WAM/STWAVE	11	0.1891	−0.0840	11	0.1544	0.0373	10	0.1204	0.0556	8	0.4037	0.6475
	SWAN	13	0.2150	−0.1031	13	0.2034	0.1265	13	0.1138	0.1177	9	0.2209	0.1364
CSI	STWAVE	4	0.1764	0.2641	4	0.1384	0.0678	4	0.1939	0.3831	0	n/a	n/a
	SWAN	5	0.1478	0.1393	5	0.1601	0.0851	5	0.2106	0.3376	2	0.2197	−0.1934
USACE-CHL	STWAVE	4	0.4252	0.4632	4	0.9701	1.1156	4	1.5295	−0.3000			
	SWAN	5	0.8827	0.7621	5	0.4844	0.2645	5	2.8319	−0.3580			
A.K.	STWAVE	8	0.2421	0.1727	8	0.1380	0.1597						
	SWAN	8	0.2892	0.1807	8	0.2156	0.1497						

Table 5. Summary of Scatter Index (SI) and Normalized Error Bias for Wave Data Time Series[a]

Data Source/ Geographic Location	Model	Sig. Wave Height			Peak Wave Period			Mean Wave Period			Mean Wave Direction		
		Number of Data Sets	SI	Bias	Number of Data Sets	SI	Bias	Number of Data Sets	SI	Bias	Number of Data Sets	SI	Bias
NDBC	***WAM/STWAVE***	11/10[b]	0.1891	−0.0840	11/10[b]	0.1544	0.0373	10/9[b]	0.1204	0.0556	8/7[b]	0.4037	0.6475
	SWAN		0.1809	0.0465		0.1725	0.0456		0.1102	0.0385		0.2449	0.0177
CSI	WAM/***STWAVE***	4	0.1951	0.2641	4	0.1384	0.0678	4	0.1939	0.3831			
	SWAN		0.1416	0.1221		0.2002	0.1343		0.2200	0.3243			
USACE-CHL	WAM/***STWAVE***	4	0.4652	0.4632	4	0.9701	1.1156	4	1.5295	−0.3000			
	SWAN		0.5201	0.8589		0.4638	0.3024		1.8304	−0.3125			
AK	WAM/***STWAVE***	8	0.2421	0.1727	8	0.1380	0.1597						
	SWAN		0.2892	0.1807		0.2156	0.1497						
Deep Water	***WAM/STWAVE***	11/10[b]	0.1891	−0.0840	11/10[b]	0.1544	0.0373	10/9[b]	0.1204	0.0556	8/7[b]	0.4037	0.6475
	SWAN		0.1809	0.0465		0.1725	0.0456		0.1102	0.0385		0.2449	0.0177
Coastal Water	WAM/***STWAVE***	12	0.2264	0.2032	12	0.1382	0.1290	4	0.1939	0.3831			
	SWAN		0.2400	0.1611		0.2105	0.1446		0.2200	0.3243			
Inland	WAM/***STWAVE***	4	0.4652	0.4632	4	0.9701	1.1156	4	1.5295	−0.3000			
	SWAN		0.5201	0.8589		0.4638	0.3024		1.8304	−0.3125			
All	***WAM/STWAVE***	27/26[b]	0.2466	0.1247	27/26[b]	0.2680	0.2378	18/17[b]	0.4499	0.0493	8/7[b]	0.4037	0.6475
	SWAN		0.2603	0.2244		0.2348	0.1308		0.5407	0.0231		0.2449	0.0177

[a]Statistics incorporate only stations that are shared between at least two model geographic coverages. Bolded and italicized model name indicates which model was active within a data set. Data sets are grouped geographically as follows: Deep Water, NDBC; Coastal Water, AK & CSI; and Inland, USACE-CHL.

[b]One station, NDBC 42007, lies within both the WAM and STWAVE model domains. Consequentially for WAM/STWAVE statistics an additional data set is used in the computation of statistics.

[63] Figure 27 indicates that there is a small low bias in southeastern Louisiana and a small high bias to the east of the storm track in southwestern Louisiana and eastern Texas. It is also important to note that the OWI H*WIND/IOKA blended winds utilized by ADCIRC are considered the best available representation of Ike's wind field, but may lack small-scale localized variations that may influence local water levels. In summary, the overall Scatter Index of 0.1463, bias of −0.0114, estimated ADCIRC HWM indicators of $R^2 = 0.91$, absolute average difference of 0.17 m (equal to 0.12 m once measured HWM error estimates are incorporated), 94% of modeled HWMs within 50 cm of measured HWMs, and standard deviation of 0.22 m (equal to 0.19 m once measured HWM error estimates are incorporated) support the accuracy of this hindcast, especially for a storm with maximum high water levels exceeding 5 m.

5. Conclusions

[64] Hurricane Ike made landfall as a strong category 2 storm at Galveston, TX. Due to Ike's large wind field and the LATEX shelf and the coast's unique geography, a number of regional and shelf-scale processes occurred before, during, and after landfall. The extensive data set collected during Ike captures the multitude of processes that occurred during Ike on the LATEX shelf and coast and provides a valuable opportunity to validate the ADCIRC, SWAN, and WAM/STWAVE models to measured data. In the deep Gulf, Ike produced significant wave heights exceeding 15 m that radiated from the storm's center and transformed upon reaching the continental shelf. At deep water NDBC stations, WAM and SWAN performed comparably for all error measures with the exception of mean wave direction for which SWAN outperformed WAM. As the swell propagates across the shelf, SWAN shows a lag in the arrival of

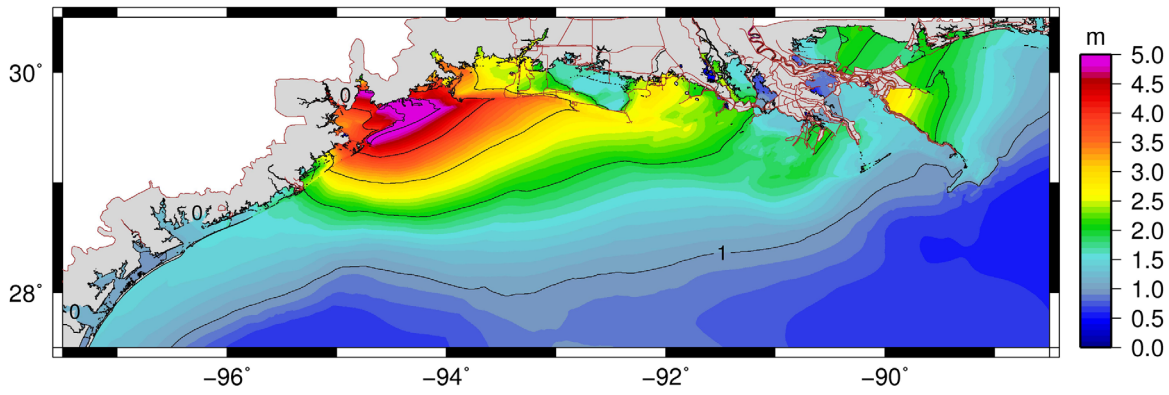

Figure 26. Extent and elevation of storm event maximum water levels (m) on the LATEX Coast during Hurricane Ike.

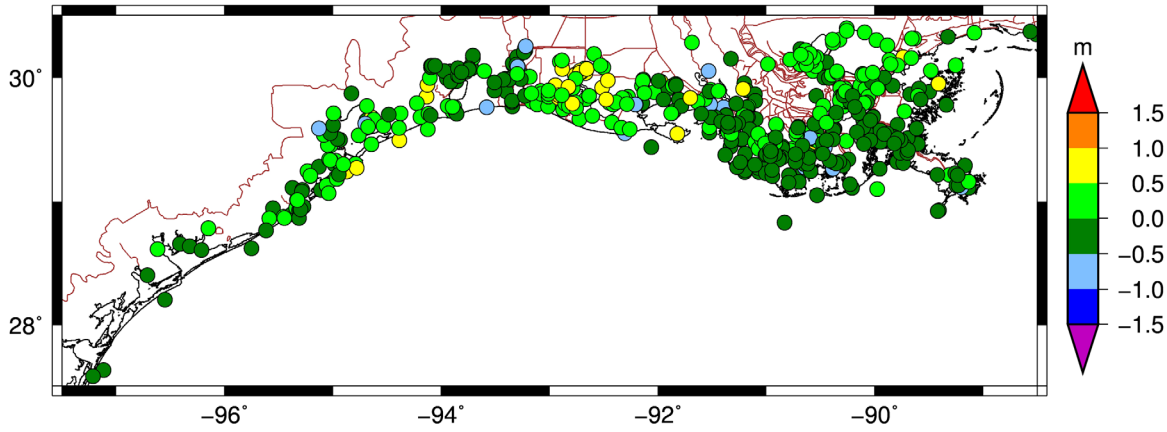

Figure 27. Spatial analysis of high water marks in Louisiana and Texas. Green represents points at which modeled water level was within 0.5 m of measured water level. Red/yellow represent points where SWAN + ADCIRC overpredicted water levels, blue/purple represent points where SWAN+ADCIRC under-predicted water levels. Coastline is in gray and SL18TX33 boundary and raised features in brown.

peak wave heights, indicating a small artificial retardation of swell on the continental shelf. This retardation has been shown to be heavily dependent on bottom friction. In the sensitivity tests, it was determined that the Madsen formulation utilized by SWAN requires the minimum Manning's n to be set equal to 0.02, avoiding unrealistically small roughness lengths. A minimum Manning n value >0.02, does not allow for accurate swell propagation. Effective wave breaking is seen in coastal marshes where wave heights are severely limited by bottom friction and shallow water column depths. Model performance in these shallow marsh areas is in a relative sense worse than in deep and coastal waters, although the waves are small here and absolute error measures are correspondingly small. However, the errors do reflect the sensitivity of waves in shallow waters to bottom friction and water levels. A thorough examination of bottom friction and its influence on wave models in shallow marsh regions would assist in better parameterizing the role of bottom friction in nearshore physical processes in wave models. The SWAN model offers a multitude of bottom friction parameterizations, of which the Madsen formulation was selected for this study based on previous success in validating Gulf of Mexico hurricanes [*Dietrich et al.*, 2011a, 2012b]. An in depth study of the model's sensitivity to other bottom friction parameterizations may provide insight into better treatment of bottom friction in complex wave environments such as those seen in Ike [*Kerr et al.*, 2013a, 2013b].

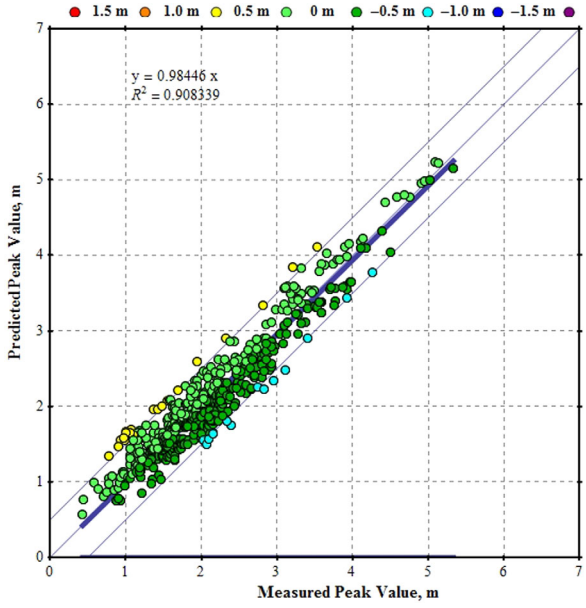

Figure 28. Scatterplot of high water marks presented in Figure 27. Y axis is modeled HWMs plotted against measured HWMs on the X axis.

[65] As Ike progressed across the Gulf, steady and moderate intensity winds over the Mississippi, Chandeleur, and Breton Sounds persisted for over 36 h. These persistent winds drove surge into the lakes, bays, and marshes surrounding New Orleans. ADCIRC's capture of the surge's growth, peak, and recession in this area indicates the model's data driven parameterization of air-sea drag and bottom friction in marsh and wetland-type areas is accurate. To the west of the Mississippi River Bird's Foot Delta, ADCIRC accurately captures the complex interaction of a strong surface water level gradient driven current, shore normal wind driven surge, and large wave breaking nearshore driven setup.

[66] The strong shore parallel current on the LATEX shelf produced by Ike's large wind field drove a forerunner surge that increased water levels at the coast and into hydraulically connected inland lakes and bays well before landfall. While this forerunner surge propagated to the southwest along the LATEX shelf and had little effect on the peak surge in open waters in Louisiana and eastern Texas, it had a significant impact on high water marks contained in hydraulically connected inland water bodies. ADCIRC captures this shelf scale process with a slight under prediction in the early rise of water at the coast, and consequently water levels lag in the coastal lakes and bays. This slight underprediction appears to be associated with a low bias in the shore parallel winds in the region during this prelandfall phase of the storm. Advection also plays a

Table 6. Summary of ADCIRC Water Levels for All Measured Water Level Data[a]

				ADCIRC to Measured HWMs					Measured HWMs		Estimated ADCIRC Errors	
Data Source	Number of Time series Data Sets	SI	Bias	Number of HWMs	Slope	R^2	Avg. Abs. Diff	Std. Dev.	Avg. Abs. Diff	Std. Dev.	Avg. Abs. Diff	Std. Dev.
AK	8	0.2409	0.0887	8								
CSI	5	0.1771	−0.0281	2								
NOAA	37	0.1137	0.0470	29	0.9710	0.9566	0.1458	0.1799				
USACE-CHL	6	0.2409	−0.0517	5								
USACE	38	0.1111	0.0133	33	0.9896	0.8842	0.1575	0.2061				
USGS-Depl	50	0.1091	0.0413	40	1.0066	0.9704	0.1710	0.2098	0.0300	0.4898	0.1410	0.2040
USGS-PERM	33	0.1086	−0.1433	24	0.9329	0.9144	0.1941	0.1938				
CRMS	321	0.1651	−0.0251	235	0.9727	0.6883	0.1785	0.2260	0.0491	0.1007	0.1293	0.2024
TCOON	25	0.1080	0.0825	17	1.0016	0.9755	0.0988	0.1246				
FEMA				206	0.9850	0.8497	0.2845	0.3575	0.1249	0.2331	0.1596	0.2711
Inland	448	0.1497	−0.0235	543	0.9790	0.8186	0.1786	0.2250	0.0511	0.1093	0.1275	0.1967
Coastal	75	0.1260	0.0606	56	1.0294	0.9426	0.1156	0.1457	0.0650	0.1216	0.0506	0.0802
All	523	0.1463	−0.0114	599	0.9844	0.9083	0.1727	0.2176	0.0524	0.1104	0.1203	0.1858

[a]Scatter index and bias were calculated for time series only. Average absolute difference and standard deviation have units of meters. To accurately determine error in measurements sets must contain at least 10 HWMs and be hydraulically connected and spatially limited. Not all time series contained usable HWM data. Inland data are defined by data sets: USACE-CHL, USACE, USGS-Depl, USGS-Perm, and CRMS. Coastal data are defined by data sets: AK, CSI, NOAA, and TCOON.

role in the forerunner generation as has been shown by *Kerr et al*. [2013a, 2013b]. Additionally, a flow regime-based bottom friction similar to that applied in riverine environments in *Martyr et al*. [2012] may further enhance the early generation of the forerunner surge.

[67] Following generation by shore parallel winds, the forerunner surge propagated down the Texas shelf as a free continental shelf wave that reached Corpus Christi as Ike made landfall. This shelf wave is modeled by ADCIRC, but slightly lags in its propagation down the coast. This is likely related to the slight low bias in the generation of the forerunner. ADCIRC also accurately represents the peak surge and positive inland water level gradient seen over the Bolivar peninsula. As Ike made landfall, maximum winds impacted inland lakes and bays that were still filled with additional water from the forerunner surge. An R^2 value of 0.91 when comparing all measured high water marks to modeled high water marks indicates ADCIRC's high level of skill in modeling peak water levels. Overall, open coastal water levels were better predicted than inland values. The large role that small-scale features and bottom friction can play in the flooding and recession processes, particularly in complex coastal marshes and wetlands warrants studies that further improve resolution in addition to improved bottom and lateral friction parameterizations.

[68] Diminishing winds following landfall allowed for the release of water driven against the coast back toward the deep Gulf. When the mass of water pushed against the coast during landfall was released by slowing winds, it was reflected by the abrupt bathymetric change at the continental shelf break resulting in a cross-shelf resonant wave with a period of 12 h. This cross-shelf resonant process is captured in ADCIRC. Surge driven into inland water bodies and coastal wetlands experienced a prolonged recession process dominated by bottom friction that occurred over a much longer time scale than the surge that developed in open water.

[69] ADCIRC's performance when compared to the wealth of data collected during the storm demonstrates this model's ability to effectively model basin and regional scale storm surge processes and the SL18TX33 computational domain's accurate portrayal of the complex LATEX shelf and coast. This performance can be quantified by an overall SI of 0.1463 and bias of −0.0114 m for 523 measured water level time series and an estimated average absolute difference of 0.12 m for 599 measured high water marks, including 94% of modeled high water marks within 0.50 m of the measured value (Figure 28 and Table 6). These qualitative assessments are similar to those found in other studies of Hurricane Ike utilizing ADCIRC and the SL18TX33 domain [*Kerr et al*., 2013a, 2013b].

[70] **Acknowledgments.** This project was supported by: NOAA via the U.S. IOOS Office (NA10NOS0120063 and NA11NOS0120141) and was managed by the Southeastern Universities Research Association; the U.S. Army Corps of Engineers New Orleans District; the Department of Homeland Security (2008-ST-061-ND0001); and the Federal Emergency Management Agency, Region 6. The National Science Foundation (OCI-0746232) supported ADCIRC and SWAN model development. Computational facilities were provided by: the U.S. Army Engineer Research and Development Center, Department of Defense Supercomputing Resource Center; The University of Texas at Austin Texas Advanced Computing Center; The Extreme Science and Engineering Discovery Environment (XSEDE), which is supported by National Science Foundation, grant OCI-1053575. Permission to publish this paper was granted by the Chief of Engineers, U.S. Army Corps of Engineers. The views and conclusions contained in this document are those of the authors and should not be interpreted as necessarily representing the official policies, either expressed or implied, of the U.S. Department of Homeland Security. The authors thank Professor Chunyan Li and the Coastal Studies Institute at Louisiana State University for providing the CSI water level and current data.

References

Amante, C., and B. W. Eakins (2009), ETOPO1 1 arc-minute global relief model: Procedures, data sources and analysis, *NOAA Tech. Memo. NESDIS NGDC-24*, 19 pp. Natl. Geophys. Data Cent., Boulder, Colo.

Battjes, J. A., and J. P. F. M. Janssen (1978), Energy loss and set-up due to breaking of random waves, in Proceedings of 16th International Conference on Coastal Engineering, Am. Soc. of Civ. Eng., Hamburg, Germany.

Battjes J. A., and M. J. F. Stive, (1985), Calibration and verification of a dissipation model for random breaking waves, *J. Geophys. Res.*, *90*(C5), 9159–9167, doi:10.1029/JC090iC05p09159.

Bender, C., J. M. Smith, A. B. Kennedy, and R. Jensen (2013), STWAVE simulation of Hurricane Ike: Model results and comparison to data, *Coastal Eng.*, *73*, 58–70, doi:10.1016/j.coastaleng.2012.10.003.

Berg, R. (2009), *Tropical Cyclone Report, Hurricane Ike, 1–14 Sep*., pp. 55, NOAA/National Hurricane Cent., Miami, Fla.

Booij, N., R. C. Ris, and L. H. Holthuijsen (1999), A third-generation wave model for coastal regions: 1. Model description and validation, *J. Geophys. Res.*, *104*(C4), 7649–7666, doi:10.1029/98JC02622.

Bretschneider, C. L., H. J. Krock, E. Nakazaki, and F. M. Casciano (1986), *Roughness of typical Hawaiian terrain for tsunami run-up calculations: A users manual, J. K. K. Look Lab. Rep*., Univ. of Hawaii, Honolulu Hawaii.

Buczkowski, B. J., J. A. Reid, C. J. Jenkins, J. M. Reid, S. J. Williams, and J. G. Flocks (2006), usSEABED: Gulf of Mexico and Caribbean (Puerto Rico and U.S. Virgin Islands) offshore surficial sediment data release, *U.S. Geological Survey Data Series 146, version 1.0*, U.S. Geol. Surv., Reston, Va.

Bunya, S., et al. (2010), A high-resolution coupled riverine flow, tide, wind, wind wave and storm surge model for southern Louisiana and Mississippi. Part I: Model development and validation, *Mon. Weather Rev.*, *138*, 345–377, doi:10.1175/2009MWR2906.1.

Cardone, V. J., and A. T. Cox (2009), Tropical cyclone wind field forcing for surge models: Critical issues and sensitivities, *Nat. Hazards*, *51*, 29–47, doi:10.1007/s11069-009-9369-0.

Cavaleri, L., and P. M. Rizzoli (1981), Wind wave prediction in shallow water: Theory and applications, *J. Geophys. Res.*, *86*(C11), 10,961–10,973, doi:10.1029/JC086iC11p10961.

Cox, A. T., J. A. Greenwood, V. J. Cardone, and V. R. Swail (1995), An interactive objective kinematic analysis system, paper presented at the Fourth International Workshop on Wave Hindcasting and Forecasting, Banff, Alberta.

Dawson, C., J. J. Westerink, J. C. Feyen, and D. Pothina (2006), Continuous, discontinuous and coupled discontinuous-continuous Galerkin finite element methods for the shallow water equations, *Int. J. Numer. Methods. Fluids*, *52*(1), 63–88, doi:10.1002/fld.1156.

Dietrich, J. C., et al. (2010), A high-resolution coupled riverine flow, tide, wind, wind wave and storm surge model for southern Louisiana and Mississippi: Part II—Synoptic description and analysis of Hurricanes Katrina and Rita, *Mon. Weather Rev.*, *138*(2), 378–404, doi:10.1175/2009MWR2907.1.

Dietrich, J. C., et al. (2011a), Hurricane Gustav (2008) waves and storm surge: Hindcast, synoptic analysis and validation in southern Louisiana, *Mon. Weather Rev.*, *139*(8), 2488–2522, doi:10.1175/2011MWR3611.1.

Dietrich, J. C., M. Zijlema, J. J. Westerink, L. H. Holthuijsen, C. N. Dawson, R. A. Luettich Jr., R. E. Jensen, J. M. Smith, G. S. Stelling, and G. W. Stone (2011b), Modeling hurricane waves and storm surge using integrally-coupled, scalable computations, *Coastal Eng.*, *58*(1), 45–65, doi:10.1016/j.coastaleng.2010.08.001.

Dietrich, J. C., et al. (2012a), Limiters for spectral propagation velocities in SWAN, *Ocean Modell.*, *70*, 85–102, doi:10.1016/j.ocemod.2012.11.005.

Dietrich, J. C., S. Tanaka, J. J. Westerink, C. N. Dawson, R. A. Luettich Jr., M. Zijlema, L. H. Holthuijsen, J. M. Smith, L. G. Westerink, and H. J. Westerink (2012b), Performance of the unstructured-mesh, SWAN+ADCIRC model in computing hurricane waves and surge, *J. Sci. Comput.*, *52*, 468–497, doi:10.1007/s10915-011-9555-6.

East, J. W., M. J. Turco, and R. R. Mason Jr. (2008), Monitoring inland storm surge and flooding from Hurricane Ike in Texas and Louisiana, September 2008, U.S. Geol. Surv. Open File Rep., 2008-1365.

Egbert, G. D., A. F. Bennett, and M. G. G. Foreman (1994), TOPEX/POSEIDON tides estimated using a global inverse model, *J. Geophys. Res.*, *99*(C12), 24,821–24,852, doi:10.1029/94JC01894.

Egbert, G. D., and S. Y. Erofeeva (2002), Efficient inverse modeling of barotropic ocean tides, *J. Atmos. Oceanic Technol.*, *19*(2), 183–204, doi:10.1175/1520-0426(2002)019<0183:EIMOBO>2.0.CO;2.

FEMA (2008), Texas Hurricane Ike rapid response coastal high water mark collection, FEMA-1791-DR-Texas, Washington, D. C.

FEMA (2009), Louisiana Hurricane Ike coastal high water mark data collection, FEMA-1792-DR-Louisiana, Washington, D. C.

Garster, J. K., B. Bergen, and D. Zilkoski (2007), Performance evaluation of the New Orleans and Southeast Louisiana hurricane protection system, Vol. II—Geodetic vertical and water level datums, Final Report of the Interagency Performance Evaluation Task Force, U.S. Army Corps of Eng., Washington, D. C., 157 pp.

Günther, H. (2005), *WAM cycle 4.5 version 2.0*, Inst. for Coastal Res., GKSS Res. Cent., Geesthacht, Germany.

Hanson, J. L., B. A. Tracy, H. L. Tolman, and R. D. Scott (2009), Pacific hindcast performance of three numerical wave models, *J. Atmos. Oceanic Technol.*, *26*(8), 1614–1633, doi:10.1175/2009JTECHO650.1.

Kennedy, A. B., U. Gravois, B. Zachry, R. A. Luettich, T. Whipple, R. Weaver, J. Reynolds-Fleming, Q. J. Chen, and R. Avissar (2010), Rapidly installed temporary gauging for waves and surge during Hurricane Gustav, *Cont. Shelf Res.*, *30*(16), 1743–1752, doi:10.1016/j.csr.2010.07.013.

Kennedy, A. B., U. Gravois, B. C. Zachry, J. J. Westerink, M. E. Hope, J. C. Dietrich, M. D. Powell, A. T. Cox, R. A. Luettich Jr., and R. G. Dean (2011a), Origin of the Hurricane Ike forerunner surge, *Geophys. Res. Lett.*, *38*, L08608, doi:10.1029/2011GL047090.

Kennedy, A. B., U. U. Gravois, and B. Zachry (2011b), Observations of landfalling wave spectra during Hurricane Ike, *J. Waterw. Port Coastal Ocean Eng.*, *137*(3), 142–145, doi:10.1061/(ASCE)WW.1943–5460.0000081.

Kerr, P. C., et al. (2013a), Surge generation mechanisms in the lower Mississippi River and discharge dependency, *J. Waterw. Port Coastal Ocean Eng.*, *139*, 326–335, doi:10.1061/(ASCE)WW.1943–5460.0000185.

Kerr, P. C., R. C. Martyr, A. S. Donahue, M. E. Hope, J. J. Westerink, R. A. Luettich Jr., A. B. Kennedy, J. C. Dietrich, C. Dawson, and H. J. Westerink (2013b), U.S. IOOS coastal and ocean modeling testbed: Evaluation of tide, wave, and hurricane surge response sensitivities to mesh resolution and friction in the Gulf of Mexico, *J. Geophys. Res.*, doi:10.1002/jgrc.20305, in press.

Kolar, R. L., J. J. Westerink, M. E. Cantekin, and C. A. Blain (1994), Aspects of nonlinear simulations using shallow water models based on the wave continuity equations, *Comput. Fluids*, *23*(3), 523–538, doi:10.1016/0045–7930(94)90017-5.

Komen, G., L. Cavaleri, M. Donelan, K. Hasselmann, S. Hasselmann, and P. A. E. M. Janssen (1994), *Dynamics and Modeling of Ocean Waves*, Cambridge Univ. Press, New York.

Komen, G. J., K. Hasselmannm, and K. Hasselmann (1984), On the existence of a fully-developed wind-sea spectrum, *J. Phys. Oceanogr.*, *14*, 1271–1285, doi:10.1175/1520-0485(1984)014<1271:OTEOAF>2.0.CO;2.

Madsen, O. S., Y.-K. Poon, and H. C. Graber (1988), Spectral wave attenuation by bottom friction: Theory, paper presented at the 21th Int. Conf. Coastal Engineering, Torremolinos, Spain.

Martyr, R. C., et al. (2012), Simulating hurricane storm surge in the lower Mississippi River under varying flow conditions, *J. Hydraul. Eng.*, *139*, 492–501, doi:10.1061/(ASCE)HY.1943–7900.0000699.

Mitchell, D. A., W. J. Teague, E. Jarosz, and D. W. Wang (2005), Observed currents over the outer continental shelf during Hurricane Ivan, *Geophys. Res. Lett.*, *32*, L11610, doi:10.1029/2005GL023014.

Mukai, A., J. J. Westerink, R. A. Luettich, and D. J. Mark (2002), A tidal constituent database for the Western North Atlantic Ocean, Gulf of Mexico and Caribbean Sea, Tech. Rep. ERDC/CHL TR-02–24, U.S. Army Eng. Res. and Dev. Cent., Vicksburg, Miss.

Powell, M. (2006), Drag coefficient distribution and wind speed dependence in tropical cyclones, Final Report to the National Oceanic and Atmospheric Administration (NOAA) Joint Hurricane Testbed (JHT) Program, Atl. Oceanogr. and Meteorol. Lab., Miami, Fla.

Powell, M. D., and T. A. Reinhold (2007), Tropical cyclone destructive potential by integrated kinetic energy, *Bull. Am. Meteorol. Soc.*, *88*(4), 513–526, doi:10.1175/BAMS-88-4-513.

Powell, M. D., S. H. Houston, and T. A. Reinhold (1996), Hurricane Andrew's landfall in South Florida. Part I: Standardizing measurements for documentation of surface wind fields, *Weather Forecast.*, *11*, 304–328, doi:10.1175/1520-0434(1996)011<0304:HALISF>2.0.CO;2.

Powell, M. D., S. H, Houston, L. R. Amat, and N. Morrisseau-Leroy (1998), The HRD real-time hurricane wind analysis system, *J. Wind Eng. Ind. Aerodyn.*, *77–78*, 53–64, doi:10.1016/S0167–6105(98)00131-7.

Powell, M. D., P. J. Vickery, and T. A. Reinhold (2003), Reduced drag coefficient for high wind speeds in tropical cyclones, *Nature*, *422*(6929), 279–283, doi:10.1038/nature01481.

Powell, M. D., et al. (2010), Reconstruction of Hurricane Katrina's wind fields for storm surge and wave hindcasting, *Ocean Eng.*, *37*, 26–36, doi:10.1016/j.oceaneng.2009.08.014.

Ris, R. C., N. Booij, and L. H. Holthuijsen (1999), A third-generation wave model for coastal regions: 2. Verification, *J. Geophys. Res.*, *104*, 7667–7681, doi:10.1029/1998JC900123.

Rogers W. E., P. A. Hwang, and D. W. Wang (2003), Investigation of wave growth and decay in the SWAN model: Three regional scale applications. *J. Phys. Oceanogr.*. *33*, 366–389, doi:10.1175/1520-0485(2003)033<0366:IOWGAD>2.0.CO;2.

Smith, J. M. (2000), Benchmark tests of STWAVE, paper presented at the Sixth International Workshop on Wave Hindcasting and Forecasting, Monterey, Calif.

Smith, J. M. (2007), Full-plane STWAVE: II. Model overview, ERDC TN-SWWRP-07-5, Vicksburg, Miss.

Smith, J. M., A. R. Sherlock, and D. T. Resio (2001), STWAVE: Steady-state spectral wave model user's manual for STWAVE, version 3.0, Tech. Rep. ERDC/CHL SR-01-1, Eng. Res. and Dev. Cent., Vicksburg, Miss.

Smith, J. M., R. E. Jensen, A. B. Kennedy, J. C. Dietrich, and J. J. Westerink (2010), Waves in wetlands: Hurricane Gustav, in *Proceedings of the 32nd International Conference on Coastal Engineering (ICCE)*, Shanghai, China.

Sorensen, R. M. (2006), *Basic Coastal Engineering*, Springer, N. Y.

Sullivan, P. P., L. Romero, J. C. McWilliams, and W. K. Melville (2012), Transient evolution of Langmuir turbulence in ocean boundary layers driven by hurricane winds and waves, *J. Phys. Oceanogr.*, *42*, 1959–1980, doi:10.1175/JPO-D-12–025.1.

Westerink, J. J., R. A. Luettich, J. C. Feyen, J. H. Atkinson, C. Dawson, H. J. Roberts, M. D. Powell, J. P. Dunion, E. J. Kubatko, and H. Pourtaheri (2008), A basin- to channel-scale unstructured grid hurricane storm surge model applied to southern Louisiana, *Mon. Weather Rev.*, *136*(3), 833–864, doi:10.1175/2007MWR1946.1.

Zijlema, M. (2010), Computation of wind-wave spectra in coastal waters with SWAN on unstructured grids, *Coastal Eng*, *57*(3), 267–277, doi:10.1016/j.coastalengsss.2009.10.011.